LEVEL II

NRL Memorandum Report 3993

Experimental Determination of the Static Properties of a Towable-VHF-UHF Horizontal Electrode Antenna

EDWIN L. ALTHOUSE, GERALD L. EPSTEIN, JEFFREY D. CHINN, AND DOUGLAS M. KOPP

Telecommunications Systems Technology
Communications Sciences Division

AD A069079

DDC
RECEIVED
MAY 29 1979
C

May 4, 1979

DDC FILE COPY

NAVAL RESEARCH LABORATORY
Washington, D.C.

Approved for public release; distribution unlimited.

79 05 25 048

SECURITY CLASSIFICATION OF THIS PAGE (When Data Entered)

REPORT DOCUMENTATION PAGE

READ INSTRUCTIONS BEFORE COMPLETING FORM

1. REPORT NUMBER: NRL Memorandum Report 3993
2. GOVT ACCESSION NO.:
3. RECIPIENT'S CATALOG NUMBER:

4. TITLE (and Subtitle): EXPERIMENTAL DETERMINATION OF THE STATIC PROPERTIES OF A TOWABLE VHF-UHF HORIZONTAL ELECTRODE ANTENNA

5. TYPE OF REPORT & PERIOD COVERED: Final report on work performed from 2/77 to 12/78

6. PERFORMING ORG. REPORT NUMBER:

7. AUTHOR(s): Edwin L. Althouse, Gerald L. Epstein*, Jeffrey D. Chinn†, Douglas M. Kopp

8. CONTRACT OR GRANT NUMBER(s): NRL-MR-3993

9. PERFORMING ORGANIZATION NAME AND ADDRESS: Naval Research Laboratory, Washington, DC 20375

10. PROGRAM ELEMENT, PROJECT, TASK AREA & WORK UNIT NUMBERS: ISCS-P-ISCAS; ED-GI64; NRL Problem R01-09A

11. CONTROLLING OFFICE NAME AND ADDRESS: Naval Electronic Systems Command, Washington, DC 20360

12. REPORT DATE: May [illegible]9

13. NUMBER OF PAGES: 60

14. MONITORING AGENCY NAME & ADDRESS (if different from Controlling Office):

15. SECURITY CLASS. (of this report): UNCLASSIFIED

15a. DECLASSIFICATION/DOWNGRADING SCHEDULE:

16. DISTRIBUTION STATEMENT (of this Report): Approved for public release; distribution unlimited

17. DISTRIBUTION STATEMENT (of the abstract entered in Block 20, if different from Report):

18. SUPPLEMENTARY NOTES: *Massachusetts Institute of Technology, Cambridge, Mass. †Tufts University, Medford, Mass.

19. KEY WORDS (Continue on reverse side if necessary and identify by block number): Trailing wire antenna; Buoyant antenna; Towed antenna

20. ABSTRACT (Continue on reverse side if necessary and identify by block number):

The static properties of impedance, radiation resistance, spatial pattern, power gain, and frequency response have been investigated for an experimental horizontal electrode antenna in the frequency range of 150 to 400 MHz. This antenna was designed to receive low data rate satellite communications with optimum performance near 250 MHz when towed near the surface of the ocean. The observed power gain and frequency response are compared to those of an experimental slot antenna borrowed from the Massachusetts Institute of Technology, Lincoln Laboratories.

(Continues)

DD FORM 1 JAN 73 1473 EDITION OF 1 NOV 65 IS OBSOLETE S/N 0102-014-6601

SECURITY CLASSIFICATION OF THIS PAGE (When Data Entered)

20. Abstract (Continued)

It was found that the electrode antenna had at resonance (250 MHz) an impedance of 170 ohms, a radiation resistance of 0.37 ohms, a power gain of −16 dBi into a 50 ohm load (−16.6 dBi into a 170 ohm load), and a 3 dB passband of about 140 MHz compared to the slot antenna's properties of −9.7 dBi static gain and 11.5 MHz passband. At incidence angles close to vertical the frequency response of the electrode antenna is described well by the expressions developed in the text.

Reference material is cited to support the contention that the dynamical performance of the electrode antenna (while in tow) cannot be accurately predicted on the basis of static measurements alone. Nevertheless, because of the 7 dB advantage in static gain that the slot antenna exhibits over the electrode antenna, it is unlikely that the electrode antenna will offer an advantage except when bandwidths much greater than 10 MHz are required.

CONTENTS

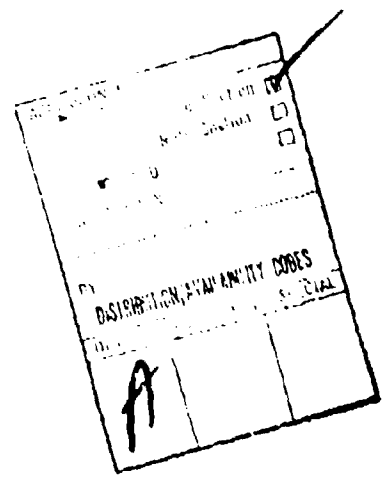

EXPERIMENTAL DETERMINATION OF THE STATIC PROPERTIES OF A TOWABLE VHF-UHF HORIZONTAL ELECTROBE ANTENNA

INTRODUCTION

Radio frequency transmissions in the VHF-UHF band that are of practical interest to submarines fall in the frequency range of 150 to 400 MHz. Short range communications, not involving satellite relays, are conducted over the entire range of 225 to 400 MHz. Communications relayed by satellites are conducted over the band of 250 to 300 MHz, and navigational information is radiated at 150 and 400 MHz. A new navigation satellite system, the NAVSTAR Global Positioning System (GPS) that will be operational by 1984, will transmit at 1228 and 1575 MHz. For reasons that will be apparent in the following material, the GPS system is too high in frequency to be useful with a buoyant cable antenna system of the type described in this report.

Communication to deeply submerged submarines in the 150 to 400 MHz band must be conducted with an antenna that is deployed above or within a few centimeters of the ocean surface because of the high attenuation rate of RF power with depth (5.5 dB/cm at 250 MHz). It is unlikely that an information rate of 1/6 bit/sec can be maintained at 250 MHz below a depth of 5 cm at towing speeds of 2 meters/sec or greater with the types of antennas considered in this report.

Although the highest data rate and greatest reliability are obtained with the antenna above the surface, a submarine on a strategic mission must maintain its covertness by minimizing the visibility of its communications antennas. This strategy may be pushed to the point where the antenna is far-removed from the submarine by means of attachment to a long buoyant transmission line or to a communications buoy towed by the submarine. The design of the antenna element can be tailored so that the minimum visibility is achieved consistent with a given performance requirement.

Candidate antennas for this application include:

(a) vertical, inclined, or horizontal elements intended for use above the surface, and

Note: Manuscript submitted March 3, 1979.

(b) horizontal elements designed for use at and below the surface.

Antennas of type (a) are usually mounted on the top surface of a buoy that is towed just below the ocean surface. Small vertical elements (spoke wheels) have also been used with moderate success at the end of a buoyant transmission line. The less visible antennas of type (b) include the horizontal electrode antenna and the slot antenna.

Horizontal electrode antennas, also referred to as trailing wire antennas, have been studied rather extensively in the past for use at frequencies below 200 MHz. Basically, such an antenna consists of a section of insulated conductor fed at one end by a coaxial transmission line. The coaxial braid of the transmission line makes electrical contact with the seawater at the feedpoint; the far end of the insulated conductor can either remain insulated or be terminated in the seawater with another electrode.

A slot antenna suitable for use near 250 MHz can be constructed using an overlapping shell of copper foil wound on an insulating core of about 1.6 cm diameter. A longitudinal slot is formed by separating the two layers of foil in the overlap region by a thin dielectric. Experimental slot antennas have been analyzed, constructed, and tested by the Massachusetts Institute of Technology, Lincoln Laboratory, (MIT-LL) [1,2].

The purpose of this report is to determine the sensitivity (static power gain), frequency response, and spatial patterns for a horizontal electrode antenna that has been optimized for performance at frequencies near 250 MHz. These characteristics will then be compared with those of a typical slot antenna in order to provide a basis for the choice of antenna types for strategic submarine communications. The static properties of an antenna are not sufficient to predict the communication performance when the antenna is towed, as is well exemplified in [1]. Therefore, complete characterization of the dynamic characteristics of the horizontal electrode antenna requires an additional experimental program involving measurements conducted with the antenna towed in an ocean environment.

The remainder of the report is grouped into a section that discusses the characteristics of the horizontal electrode antenna, including physical description, impedance, spatial pattern, power gain, and frequency response; a section that discusses measurement technique; and sections that present the results and conclusions.

CHARACTERISTICS OF THE HORIZONTAL ELECTRODE ANTENNA

Physical Description

A photograph of the antenna constructed for the experiments is shown in Fig. 1. The components are identified as:

T: RG-214 coaxial transmission line

E: Ring-shaped metallic electrode that is electrically connected to the shield of the transmission line

I: Dielectric insulating material (Emerson and Cuming ECCOFOAM FP closed cell polyurethane foam)

N: Coaxial nylon rod that extends inside the antenna to the point E.

The internal construction of the antenna is shown in Figs. 2 and 3, which show the components assembled in one half of the aluminum mold used to cast the polyurethane foam insulating jacket. From point A (Fig. 2) to the ring electrode the nylon rod is reduced in diameter from 1.27 cm to 0.95 cm and is covered with several layers of 0.005 cm thick copper foil, which is soldered to a splayed nest of wires from the stranded center conductor of the transmission line. A closer view of this area is given in Fig. 3. The spacers are made from precast sheets of polyurethane foam of the same composition as used in the final cast. The overall length of the antenna is 76 cm, the length of the inner copper foil element is 37.5 cm, and the diameter of polyurethane foam jacket is 3.18 cm. The use of a cylindrical shell conductor instead of a simple extension of the central conductor of the transmission line results in a lower antenna resistance (170 ohms) at resonance. Reduction of the resistance at resonance to the vicinity of 50 to 75 ohms, a desirable range from the standpoint of matching to transmission lines and amplifiers, requires a substantial increase in diameter of the inner copper foil element. No attempt was made to construct a 50 ohm antenna since there was an a priori decision to limit the overall diameter to 3.18 cm. Decreasing the thickness of the insulating foam jacket in order to accommodate a larger diameter for the inner element would have resulted in a lower antenna efficiency.

Impedance

The input impedance of the horizontal electrode antenna can be calculated by analyzing the antenna configuration as a lossy coaxial transmission line. The seawater, which acts as the outer coaxial conductor, is characterized by a complex dielectric constant that can be calculated from the conductivity and relative dielectric

constant of the medium. The analytical procedure is documented in detail by Flath and Norgorden [3] and, in somewhat less detail, by Fessenden and Cheng [4] , and Fenwick and Weeks [5]. Strictly speaking, this procedure for calculating impedance is valid only when the antenna is fully submerged in the water, but, as will be seen from actual measurements presented under RESULTS (Figs. 11 and 12) is sufficiently accurate near the surface.

A computer program was written using the formulation of Flath and Norgorden to compute the frequency dependence of the impedance for the horizontal electrode antenna. The results are shown in Fig. 4 using the physical dimensions previously given for the antenna, a dielectric constant of 1.8 for the polyurethane foam, and a conductivity of 4.2 mho/m for the water.

Spatial Pattern

Figure 5 shows the relationship of the perpendicular field components E_θ and E_ϕ to the coordinate system used in this report. The E-field vector of a wave incident with plane polarization can be completely resolved into E_θ and E_ϕ components. A horizontally polarized wave will have only an E_ϕ component, and a wave with polarization in the plane of incidence (vertical plane polarization) will have only an E_θ component.

Mathematical expressions for the variation of the electric field strength with distance and direction in the far field above the sea surface have been derived by Bigge [6] and Bigge and Swarm [7] for a submerged horizontal dipole of infinitesimal length. The expressions for E_θ and E_ϕ were integrated over the 37.5 cm antenna length using the current distribution given by Fenwick and Weeks [5] for an end-fed antenna. The integrations were carried out numerically on the NRL ASC (Texas Instruments) computer using double precision arithmetic (64 bit accuracy). These computations were used to determine the gain patterns that are plotted along with the measured data presented under RESULTS.

Numerical values of the theoretically calculated normalized field constants $[rE_\theta/I]^2$ and $[rE_\phi/I]^2$ are presented in Table 1. The magnitude (in volts/m) of E_θ or E_ϕ produced by the antenna at a distance r by a feedpoint current I is given by multiplying the field ratio implied by a given entry in Table I by the value of I/r (in amps/meter). An asymmetry exists for the E_θ pattern in the $\phi = 0^\circ$, 180° directions because the antenna is end-fed; this effect becomes more significant as the frequency is increased.

TABLE 1 - E-FIELD RADIATION CONSTANTS FOR ELECTRODE ANTENNA

$[rE_\theta/I]^2$ (dB//1 Volt/Amp)

	200 MHz		250 MHz		400 MHz	
θ	(φ=0)	(φ=180)	(φ=0)	(φ=180)	(φ=0)	(φ=180)
0	14.40	14.40	21.06	21.06	7.78	7.68
15	14.25	14.44	20.74	21.23	4.36	11.37
30	14.00	14.39	20.31	21.26	6.94	13.76
45	13.68	14.22	19.78	21.13	8.65	15.11
66.4	13.01	13.73	18.86	20.62	10.23	15.63
85.7	9.68	10.46	15.14	17.05	6.67	11.75

$[rE_\phi/I]^2$ (dB//1 Volt/Amp)

	200 MHz	250 MHz	400 MHz
θ	(φ=90, 270)	(φ=90, 270)	(φ=90, 270)
0	14.40	21.06	7.68
15	14.11	20.77	7.30
30	13.19	19.85	6.32
45	11.49	18.15	4.57
66.4	6.64	13.32	-0.29
85.7	-7.81	-1.12	-14.72

Radiation Resistance

The radiation resistance R_r of the horizontal electrode antenna was determined by integrating the E_θ and E_ϕ field constants over 4 π steradians:

$$R_r = \frac{1}{120\pi} \int_{\phi=0}^{2\pi} \int_{\theta=-\pi/2}^{\pi/2} \left\{ [rE_\theta(\theta,\phi)/I]^2 + [rE_\phi(\theta,\phi)/I]^2 \right\} \sin\theta \, d\theta \, d\phi \quad (1)$$

In Eq. (1) the antenna is assumed to be lying on the ocean surface so that the fields vanish over the lower half space. Recognition of the factor of 120 π as the impedance of free space is necessary to obtain the dimensions of resistance. The validity of Eq. (1) can be demonstrated by the following line of reasoning. The total power W radiated by the antenna with feedpoint current I is given by

$$W = I^2 R_r, \tag{2}$$

substituting Eq. (1) into Eq. (2) gives

$$W = \frac{r^2}{Z_o} \int_{\text{all } \theta,\phi} \left(E_\theta^2 + E_\phi^2 \right) \sin\theta \, d\theta \, d\phi = 4\pi r^2 \frac{\overline{E_\theta^2 + E_\phi^2}}{Z_o} = 4\pi r^2 \bar{P} \tag{3}$$

where Z_o is the impedance of free space, the quantities with a bar above represent averages over 4π steradians, and P is the power flux density. Hence, our definition of R_r in Eq. (1) produces the correct and fundamental relationship $P = W/4\pi r^2$ as required.

The integration implied in Eq. (1) was performed numerically on a computer using 42 values of E_θ (evenly spaced in θ from $\pi/2$ to 0) and 74 values of E_ϕ (evenly spaced in ϕ from 0 to π) for each frequency considered. The integration over ϕ from π to 2π is identical to that from 0 to π from symmetry and the integration over θ from 0 to $-\pi/2$ was ignored since E_ϕ and E_θ are assumed to vanish. The computed values of radiation resistance are shown in Table 2 and are accompanied by tabulations of the experimentally determined resistance (primarily loss resistance R_l) and reactance X. The fact that the radiation resistance and the antenna gain maximize near 250 MHz indicates that the best antenna performance will be achieved in this region provided the characteristic impedance of the transmission line matches the antenna impedance of 170 ohms.

Power Gain and Frequency Response

We will define the power gain of the antenna as the quotient of the directive (or lossless) gain G_d (relative to isotropic) and the loss factor L associated with the impedance mismatch of the antenna and load

$$G_p(\theta,\phi) = G_d(\theta,\phi)/L \tag{4}$$

where

$$L = \frac{R_r + R_l + R_L)^2 + X_a + X_m)^2}{4 R_r R_L} \tag{5}$$

and R_L is the load resistance, X_a is the antenna reactance, and X_m is any other residual reactance (possibly introduced to provide impedance matching) in the equivalent circuit of the antenna, transmission line, and load. The loss factor L does not include any losses incurred on the transmission line.

From reasoning similar to that used in consideration of radiation resistance, it can be shown that the directive gain is given by

$$G_d(\theta,\phi) = [rk(\theta,\phi)/I]^2/30\ R_r \qquad (6)$$

Table 2 - IMPEDANCE AND RADIATION RESISTANCE OF ELECTRODE ANTENNA

FREQUENCY (MHz)	RADIATION RESISTANCE † (ohms) R_r	LOSS RESISTANCE * (ohms) R_ℓ	REACTANCE * (ohms) X
150	.0158	28.3	25.0
175	.0348	43.5	51.0
200	.0821	73.0	76.0
220	.173	130.0	58.0
250	.372	170.0	-2.5
265	.318	163.0	-71.0
280	.217	133.0	-82.0
310	.102	57.0	-63.0
340	.0605	42.0	-36.0
370	.0471	37.7	-10.0
400	.0487	40.5	5.0

† CALCULATED

* MEASURED

where the quantity in brackets has been defined previously by a field constant of the antenna, and values have been tabulated in Table 1. The power gain of the antenna is then given by

$$G_p(0,\phi) = [rE(0,\phi)/I]^2/30\ R_r L \quad . \tag{7}$$

The frequency dependence of G_p is calculated most easily on a point-to-point basis by inserting in Eq. (7) calculated values of $[rE/I]$, R_r, and L at discrete frequencies. The power observed at the load is proportional to the product of the power gain and the maximum effective aperture of an isotropic antenna $\lambda^2/4\pi$ and consequently exhibits a dependence of (frequency)$^{-2}$ in addition to the frequency dependence implicit in Eq. (7).

MEASUREMENTS

Outdoor Measurement Range

The measurements of spatial pattern, power gain relative to isotropic, and frequency response were conducted at the NRL Test Facility located at Brandywine, Maryland. This facility consists of a 305 meter diameter ground plane constructed from galvanized hardware cloth, an underground building for instrumentation near the center of the ground plane, and a 4.6 meter diameter platter that can be rotated and lowered below ground level by a hydraulic system. A 1.22 meter x 1.83 meter 0.20 meter deep wooden tank with plastic liner was placed at the center of the platter and a raised plywood base covered with a hardware cloth ground screen was constructed around the tank.

During the experimental measurements, the platter was lowered so that the water level in the tank and the ground screen over the platter were in the same horizontal plane as the outer ground screen. The two ground screens were electrically connected to each other. A photograph of this setup is shown in Fig. 6 with the horizontal electrode antenna floating half submerged in the tank and an AT-150/SRC broadband dipole, used for transmitting a test signal, secured to a telephone pole. This setup was used to measure the power gain and frequency response of the antenna in the tank with the polarization of the incident radiation in the vertical plane. The distance between the two antennas was 9.67 meters, the angle of arrival of energy at the receiving antenna relative to the vertical was 66 degrees, and the axis of the AT-150 dipole was oriented perpendicular to a straight line connecting the two antennas. The ground screen was extended around the raised lip of the tank and into the salt water (conductivity adjusted to approximately 4.2 mho/m) to assure proper electrical continuity to the composite ground plane. The perturbation of the ground plane by the raised lip of the tank may cause some distortion to the measured antenna power gain, particulary at low angles relative to the horizontal.

A similar setup is shown in Fig. 7 for measurement of the power gain of a slot antenna borrowed from MIT-LL. The slot antenna is oriented so that the incident E-field is perpendicular to the axis of the slot as required for maximum sensitivity with polarization in the vertical plane. An adjustable monopole antenna mounted on an aluminum ground plane is shown just beyond the far side of the tank. The monopole was adjusted to quarter wavelength (trimming was performed by observing the impedance with a General Radio network analyzer) at several frequencies to determine the the power gain of the AT-150 transmitting dipole. The monopole and aluminum ground plane were not present when measurements were made on the antenna in the tank.

In Fig. 8 a picture is shown of the setup for making power gain measurements on the slot antenna with the incident polarization in the horizontal plane. The horizontal electrode antenna is oriented 90° relative to the slot antenna for similar measurements.

In order to determine the power gain of the horizontal electrode and slot antennas at an arrival angle closer to normal incidence, the AT-150 transmitting dipole was hoisted by a rope and pulley suspended between two telephone poles to a position 16 degrees from vertical at the center of the tank (see Fig. 9). The distance between antennas was 17.7 meters, and the polarization was horizontal.

The pattern measurements were made with the setup shown in Fig. 10. A rope line which moved on a pulley system was used to change the position of a battery operated transmitting dipole from an aspect of near grazing incidence to directly overhead. The movable rope line was inclined at approximately 45° and was supported above in a pulley secured to a heavy rope line between two 18 meter height telephone poles. The distance of closest and most distant approach of the transmitting and receiving antennas were 8.5 and 12.0 meters, respectively.

The position of the transmitting antenna was determined by measuring the elevation angle and bearing with a theodolite mounted on a tripod. A computer program was used to convert the theodolite readings into propagation distance and arrival angle at the receiving antenna.

The portable transmitting dipole was constructed from two aluminum mini-boxes that were modified to permit an electrically insulated mounting on a rectangular bakelite block at the center (feedpoint) and to accept 0.64 cm thick aluminum blocks at the outside ends that had threaded holes to accept 1/4"-20 threaded brass rods for adjustment of antenna length. One minibox contained a battery pack, and the other contained the oscillator and driver

electronics module (Hope Electronics model XO-10/V724). When the oscillator modules were changed to alter the frequency, new brass rod antenna ends were installed to achieve approximate half-wavelength antenna characteristics.

The range was calibrated by replacing the antenna under test by the adjustable monopole antenna mounted on the large aluminum ground plane previously shown in Fig. 7. The aluminum ground plane was cut to fit snugly inside the tank and to achieve good electrical contact with the surrounding hardware cloth ground plane. The salt water was removed from the tank for the calibration measurements. The monopole was trimmed at each frequency to a quarter wavelength by observation of its impedance with the network analyzer. The method used to relate the gain of the antenna under test to the gain of an isotropic antenna will be discussed subsequently.

Measurement Techniques

All RF measurements were made in the underground instrumentation room. A source substitution method was used to determine the received RF carrier power level. A Scientific Atlanta receiver was used to determine a relative indication of RF power level from the receiving antenna. This relative level was then determined absolutely, immediately after each measurement point, by substituting the signal with a matching output from a 50 ohm RF signal generator. The output level of the RF signal generator was then determined with a Boonton model 92AB RF millivoltmeter.

A difficulty encountered with this method was that the Scientific Atlanta receiver did not exhibit a 50 ohm impedance at all frequencies as had been initially assumed. Use of the network analyzer at the input connector of the receiver showed that a VSWR of 3:1 existed at some frequencies. The VSWR introduced by the receiver mismatch to the RG-214 transmission line (connected to the receiving antenna) and to the shorter, but more lossy, RG-58 transmission line (connected to the substitution RF generator) caused variations of a few dB from reading to reading as the frequency was changed. This effect was reduced to an insignificant level by inserting a precision coaxial 10 dB attenuator between the transmission line and the input of the Scientific Atlanta receiver. The VSWR measured at the 10 dB attenuator when connected to the receiver was less than 1.2:1; hence the additional power loss on the transmission lines caused by the receiver VSWR was eliminated. Unfortunately, this problem and its remedy were discovered after the measurements were completed with the AT-150 transmitting dipole mounted on the telephone pole (low aspect measurements, θ = 66 degrees). The measurements with the AT-150 dipole hoisted to a high aspect angle (θ = 16 degrees) were made using the attenuator, and the reduction in scatter of the data points taken every 5 MHz in frequency was substantial.

The matched loss on each transmission line was determined by measuring the power loss between input and output of the line when driven by a 50 ohm impedance RF signal generator. The additional loss from impedance mismatch of the slot antenna, horizontal electrode antenna, or AT-150 transmitting dipole was determined from impedance measurements on the transmission lines with the antenna of interest connected and placed in its intended position for range measurements. The VSWR at the generator (network analyzer) was calculated from [8]

$$VSWR_g = \frac{1 + |\Gamma|}{1 - |\Gamma|} \tag{8}$$

where

$$|\Gamma| = \sqrt{\frac{(a-1)^2 + b^2}{(a+1)^2 + b^2}} \tag{9}$$

and

$$\begin{aligned} a &= |Z| \cos(\angle Z)/50 \\ b &= |Z| \sin(\angle Z)/50 \end{aligned} \tag{10}$$

and $|Z|$ and $\angle Z$ are the magnitude and phase angle of the complex impedance as read from the network analyzer. The factor of 50 in Eq. (10) normalizes the expressions to the 50 ohm characteristic impedance of the transmission lines. The VSWR at the load end (at the antenna) of the line was calculated from

$$VSWR_\ell = \frac{1 + R_g L}{1 - R_g L} \tag{11}$$

where R_g, the reflection coefficient at the generator, is given by

$$R_g = \frac{VSWR_g - 1}{VSWR_g + 1} \tag{12}$$

and L is the matched loss of the line. The total loss of the line in dB was then calculated from

$$L_t(dB) = 10 \log \left[\frac{L^2 - R_\ell^2}{L(1-R_\ell^2)} \right] \tag{13}$$

where R_ℓ, the reflection coefficient at the load, is given by

$$R_\ell = \frac{VSWR_\ell - 1}{VSWR_\ell + 1} \tag{14}$$

Determination of the power gain relative to isotropic G_i of the antenna under test using the AT-150 dipole as a radiator was determined as follows. The power received P'_r on a 50 ohm load directly at the terminals of the receiving antenna is given by

$$P'_r = \frac{P'_o G_D}{4\pi r^2} \left(\frac{\lambda^2}{4\pi}\right) G_i \qquad (15)$$

where P'_o is the power delivered to the transmitting antenna, G_D is power gain of the transmitting antenna, r is the distance between antennas in meters, $\lambda^2/4\pi$ is the maximum effective aperture of an isotropic receiving antenna, λ is the free space wavelength, and G_i is the power gain of the receiving antenna relative to isotropic. Solving Eq. (15) for G_i and expressing λ in terms of frequency gives

$$G_i = \frac{P'_r r^2 f^2(\text{MHz})}{P'_o G_D} \left(\frac{4\pi}{300}\right)^2 \qquad (16)$$

Equation (16) can be related to the transmitted and received power levels at the far end of the transmission line by

$$P'_r = 10^{(P_r+L_r)/10}$$

$$P'_o = 10^{(P_t-L_t)/10} \qquad (17)$$

where P_r is the power measured at the end of the receiving transmission line with total loss L_r, and P_t is the power delivered by the signal generator to the input of the driving transmission line with total loss L_t. The quantities P_r, L_r, P_t, and L_t are expressed in dB.

For the pattern measurements using the self-contained battery-powered dipole radiator, the gain of the antenna under test was determined by the following method. The gain of the antenna under test at a given frequency, polarization, and incidence angle can be determined by

$$G_i = P_i - P_m + G_m \qquad (18)$$

(all quantities in dB)

where P_i is the power received by the antenna under test, P_m is the power received by a quarter wavelength monopole under identical conditions and G_m is the gain of the monopole relative to isotropic.

The procedure followed was to plot the power received by the monopole antenna as a function of incidence angle at the receiving antenna (see Figs. 19, 23, and 28 for actual data). These plots show deviations from the response that would be obtained if there were no perturbations to the range such as the raised lip of the test tank. The distribution of power versus incidence angle that would have been obtained in the absence of the perturbations to the ground plane was calculated using antenna theory. As the transmitting dipole is moved along the inclined rope line of the test range, the power received by the monopole will change because of the changing aspect relative to both the transmitting and receiving antennas and because of the changing separation between them. Proper mathematical treatment of these variables will produce a distribution of power versus incidence angle that is correct in a relative sense but often inaccurate in an absolute sense; hence it was necessary to scale the calculated distribution in power until good agreement was obtained with the measured data (see Figs. 19, 23, and 28 for examples). The difference between the measured and calculated distribution is the only means available for estimating the deviation of the monopole gain from ideal.

In Eq. (18) one could use the actual measured values of P_m with values of G_m determined from the gain of an ideal monopole with a correction factor that accounts for the deviation of monopole gain from ideal. This factor will be a function of incidence angle. A simpler and equivalent method (the method used by the authors) is to use values of G_m based on an ideal monopole without correction factors and to use values of P_m as determined from the calculated response scaled for best agreement with the measured data.

The reasoning given above may be restated as follows. The relative shape of the gain pattern of the antenna under test is determined from (a) the measurements of the power received on this antenna as a function of incidence angle and (b) the calculation of the relative distribution of power that would be received on an ideal monopole antenna as a fucntion of incidence angle. The absolute gain of the antenna under test is determined from measurements on both antennas. Calculations had to be used to eliminate the effect of ground plane perturbations on the gain pattern of the monopole antenna; there was no alternative to this procedure without a major restructuring of the test facility.

The values of G_i determined in this manner for the horizontal electrode antenna are influenced by the perturbations to the ground plane by the lip of the test tank. However, it should be realized that the effect of imperfection of the ground plane will be different for the electrode antenna than for the monopole because of the greatly different current distributions involved.

No corrections for additional loss from VSWR on the receiving transmission line were used in these measurements because they were intended primarily to measure the spatial pattern for which relative measurements are sufficient. Absolute accuracy also suffered from battery drift, substitution of new batteries between different measurement runs, and the passage of time (days) between measurement of P_i and P_m. Generally, the power gains determined from these measurements support the measurements made with the more accurate method using a signal generator to drive the AT-150 dipole via a transmission line.

RESULTS

Impedance

The frequency dependence of the impedance of the electrode antenna was measured in the laboratory in a fiberglass cylindrical tank of 1.25 meters diameter and 0.76 meters height containing salt water having a conductivity of 4.12 mho/m. The impedances reported have been transformed to correspond to the actual impedance at the antenna end of the one meter length transmission line used to connect to the probe of the network analyzer. The antenna was secured by strings to hold it near the center of the tank during the measurements, and small movements about the tethered position did not affect the measurements.

In Fig. 11 the impedance is shown as a function of frequency for the antenna submerged deeply in the water. The resonance occurs at approximately 250 MHz with a resistance of 165 ohms. In Fig. 12 the impedance is shown for the antenna floating horizontally on the surface with approximately three fifths of the antenna cross-section submerged. The impedance change between this state and the fully submerged state is insignificant. The measured impedances in Figs. 11 and 12 are in excellent agreement in magnitude and frequency dependence with the theoretical calculations presented previously in Fig. 4.

The effect on impedance of antenna bobbing as it is (hypothetically) towed along a rough ocean surface is presented in Figs. 13 and 14. In Fig. 13 the antenna is tipped 5 degrees off the horizontal such that half of the inner insulated conducting element is below the surface and half is above, while the ring electrode is submerged. In this case the resonance has shifted upward in frequency about 1 MHz, and there is a small shift in the relative amplitude of the reactive maxima. In Fig. 14 the antenna is tipped 19 degrees off the horizontal, again maintaining half of the inner conductive element submerged and the remaining half above the surface. In this case the resonance shifts upward almost 45 MHz. The corresponding change in impedance at 250 MHz would result in a 3 dB decrease in

sensitivity (neglecting any additional losses from VSWR) if the receiving amplifier were matched to the 170 ohm impedance characteristic of an untipped configuration.

Power Gain and Frequency Response

The frequency response and power gain determined for the horizontal electrode antenna and slot antenna (identified as antenna No. 2, p. 78, reference [1]) for horizontal polarization at an incidence angle of 16 degrees with respect to the vertical are shown in Fig. 15. The experimental setup was shown previously in Fig. 9, and the experimental procedure was discussed in the last section.

The static gain of the slot antenna was determined to be -9.4 dB relative to isotropic (hereafter abbreviated dBi), in close agreement with the value of -9.7 dBi reported in [1]. The maximum gain of the horizontal electrode antenna was -18 dBi, but the bandwidth of this antenna is at least ten times greater than that of the slot antenna. The impedance of the horizontal electrode antenna (170 ohms at 250 MHz, see Fig. 12 or Table 2 for values at other frequencies) was not matched to the 50 ohm characteristic impedance of the transmission line; consequently, it is possible to improve the power gain of this antenna by about 1.5 dB at a particular frequency by use of a stub tuner or impedance transformer. Hence, at this angle of incidence, the maximum power gain possible with the horizontal electrode antenna is 7 dB worse than that achieved with the slot antenna.

The systematic undulations of the data points determined for the horizontal electrode antenna are believed to be caused by the combined effect of the frequency dependent impedance mismatch of the antenna and the impedance transformation characteristics of the 11.03 meter length of transmission line. The effects of the matched loss of the transmission line and the additional loss caused by standing waves have been eliminated from the data in Fig. 15 by the method described in the previous section.

The data points indicated by squares and connected by straight line segments represent the variation of power gain calculated by Eq. (7) at a few discrete frequencies. The agreement in magnitude and frequency response between the measured and calculated data is very satisfactory.

The determination of power gain as a function of frequency at an incidence angle of 66° (with respect to vertical) is shown in Fig. 16 for polarization of the incident wave in the vertical plane. As discussed in the previous section, these measurements show considerably more scatter from point to point because of an additional impedance mismatch to the transmission line at the input

to the Scientific Atlanta receiver. Straight line segments have been drawn between high-lying data points and also between low-lying data points in order to facilitate visualization of the frequency dependence.

The maximum gain of the slot antenna at this aspect was determined to be -8.8 dBi, which is 0.9 dB higher than the value reported in [1]. The lower angle of incidence (closer to horizontal) should result in about 1 dB decrease in gain (to about -10.7 dBi) according to the data on p. 36 of [1]. Hence, our measurement of gain for the slot antenna shows about +1.9 dB disparity with the value expected from the MIT-LL data.

Table 1 shows that theoretically the gain of the horizontal electrode antenna should decrease about 2 dB as the angle of incidence is changed from 16° to 66° for polarization in the vertical plane. The measured value at 66° incidence is 2.8 dB less than at 16° incidence giving reasonable agreement with theory; however, many adjacent points lie considerably lower, probably because of impedance mismatch with the Scientific Atlanta receiver.

The agreement of the power gain calculated from Eq. (7) with measured values is poor in comparison to that shown in Fig. 15 particularly in the vicinity of 340 MHz where a broad minimum appears in the response. A plausible explanation for this effect, which is reinforced by measurements of antenna pattern, is that a reflection of the incident wave occurs at the edge of the salt water tank and travels as a surface wave back to the antenna where it reinforces or diminishes the direct wave.

This situation is shown in Fig. 17 in which the antenna is indicated between points F and G and the perturbation of the ground plane caused by the lips of the salt water tank is shown at points R and Q. The possibility of producing a reflection at point Q originates from the raised vertical conducting lip of the wall (3.8 cm high) and from the discontinuity in conductivity and dielectric constant of the ground plane at the same point. Ray BQ is reflected at point Q, and the reflected wave is assumed to propagate to the antenna as a surface wave. Since the polarization is in the vertical plane, negligible phase shift is expected at the reflection at point Q. The surface wave propagates with the E vector tipped forward, so that if the secondary path PQO is an integral number of wavelengths the horizontal components of the direct wave E and the reflected wave E' at point O will interfere destructively. Constructive interference arises when the path length PQO is an odd multiple of half wavelengths.

The frequencies of maximum constructive or destructive interference can be predicted from the geometry of the setup. The length of the path PQO, given by L (1 + sin θ) where L is one half the distance of RQ, is computed in terms of fractional wavelength of the incident wave. The frequencies at which extremes in the interference arise are calculated from

$$f(\text{MHz}) = 300\ g/L\ (1 + \sin\theta) \qquad (19)$$

where g is the fractional wavelength. For the value of L = 0.914 m appropriate to our measurements, interference extremes are located as shown in Table 3.

Table 3

g	1.50	2.00	2.50
effect	+	−	+
f(MHz)	257	342	429

+: constructive interference

−: destructive interference

The frequencies given in Table 3 are in qualitative agreement with the anomolous behavior of the data of Fig. 16. The interference minimum predicted at 342 MHz coincides with the minimum in the data; the interference reinforcements which are predicted at 257 and 429 MHz appear to occur in the data near 230 and 395 MHz.

Although the agreement between the predictions and the data is not exact, it is close enough to add credence to the hypothesized mechanism of interference. This hypothesis will be further supported with regard to its effect on measured antenna patterns.

In Fig. 18 the power gain and frequency response are shown for horizontal polarization at an incidence angle of 66°. From the MIT-LL data [1] the maximum gain of the slot antenna is expected to decrease to -17.7 dBi, and we observe a value of -19.0 dBi. From our pattern calculations, the gain of the horizontal electrode antenna near 250 MHz should decrease about 7.2 dB to a value of -25.6 dBi; however, we observed a value of -30 dBi, suggesting a possible measurement error of -4.4 dB.

Lines have been drawn rather arbitrarily between high-lying data points and also between low-lying data points in order to facilitate visualization of the frequency dependence of the data. While there is again a rather large disparity between the measured points and the theoretical response, the variation is not as pronounced as in Fig. 16. If an interference effect is present in this measurement, it cannot be caused by a surface wave because it is unlikely that one would be generated by a horizontally polarized incident wave, and the receiving antenna would be insensitive to it because of its orientation.

Reflections from the tank lip in the form of nearly horizontally traveling waves with horizontal polarization would be expected to have less effect than in the vertical polarization case because of the much lower antenna gain near grazing incidence. Nevertheless, if Eq. (19) is applied with L = 0.572 (appropriate to one half the short dimension of the tank), a subtractive interference is predicted at 274 MHz and an additive interference at 411 MHz -- again in qualitative agreement with the observations. Direct reflection from the front lip of the tank would produce a subtractive interference that would be relatively independent of frequency over the band of interest. However, a similar effect should exist in the measurements of antenna pattern for horizontal polarization and would produce a pattern depression near $\theta = 90^{\circ}$ at 250 MHz and a pattern elevation near $\theta = 75^{\circ}$ at 400 MHz. Since no anomalies were observed in any of the horizontal patterns (data are presented subsequently), it is not very likely that interference from reflections is the source of the discrepancy between theory and measurement in Fig. 18.

Spatial Pattern

The physical setup for the pattern measurements and the method used to determine the power gain were described in the last section. Fig. 19 shows the power received at 257.5 MHz on a quarter-wave monopole used for calibration and the response curve (solid line) calculated for the system on the basis of the relative positions and textbook patterns of a transmitting dipole antenna and receiving monopole antenna.

These data were applied to measurements of power received on the horizontal electrode antenna to obtain the power gain pattern (Fig. 20) in a vertical plane coincident with the antenna axis ($\phi = 0$). The solid curve drawn through the data points is the pattern calculated theoretically using the spatial field expressions given in [6] and the current distribution given in [5], as discussed briefly under CHARACTERISTICS OF THE HORIZONTAL ELECTRODE ANTENNA. The agreement between the theoretical and measured pattern is excellent except beyond $\theta = 70^{\circ}$ where more power is measured than

predicted. A possible explanation for this anomolous behavior is the existence of interference between the incident wave and a surface wave generated from a reflection of the incident wave at the far edge of the salt water tank. This hypothesis has been discussed previously in regard to Fig. 16.

If Eq. (19) is rearranged and used to solve for the angle θ for which the hypothesized interference either reinforces ($g = 0.5$) or diminishes ($g = 1.0$) the direct wave, a reinforcement is predicted at $\theta = 76^\circ$ and a diminishment at $\theta = 18^\circ$. It is unlikely that a reflection with significant power will be produced at $\theta = 18^\circ$ because the angle of incidence is nearly vertical; correspondingly, no effect is observed near 18° in Fig. 20. At an incidence angle of 76° reflection at the edge of the tank is likely to be a stronger effect, and indeed the measured power levels exceeded the theoretical estimates at $\theta = 76^\circ$. Since the fractional wavelength parameter g increases from 1.5 λ at 76° to only 1.52 λ at 90°, the reinforcement effect of the interference will be strong out to $\theta = 90^\circ$.

Figure 21 shows the power received on a horizontal halfwave dipole elevated 0.23 λ above an aluminum ground plane in the test tank. The polarization of the transmitting antenna was horizontal. The solid curve is the distribution calculated on the basis of the relative positions of the antennas, a textbook dipole pattern for the transmitting antenna, and a pattern calculated for the elevated dipole using the Fresnel reflection coefficients (p. 630 of [8]) for a good conductor.

These data were combined with measurements of power received with horizontal polarization on the electrode antenna at 257.5 MHz in a vertical plane perpendicular to the axis of the antenna ($\phi = 90^\circ$). The result is shown in Fig. 22 and is in excellent agreement with the theoretical calculation (solid curve). The power gain at zero degrees incidence should be identical in Figs. 20 and 22; however, a measurement error of about 2 dB is noted.

Figures 23 to 25 show the results of measurements taken with vertical polarization at 250 MHz. Again, the measured patterns at $\phi = 0^\circ$ (Fig. 24) and $\phi = 45^\circ$ (Fig. 25) agree relatively well with the theoretical pattern at incidence angles less than 70°. Above 70° the hypothesized interference effect may be responsible for the excess measured power.

Figures 26 and 27 show the patterns for horizontal polarization at 250 MHz at $\phi = 90^\circ$ and $\phi = 45^\circ$. For these patterns, and for all subsequent horizontal polarization pattern determinations, an elevated horizontal dipole was not used to calibrate the range because of the cumbersome procedure of constructing a properly

trimmed and balanced antenna for each new frequency. Instead, the power incident at the electrode antenna was obtained by calculation based on the relative positions of the transmitting and receiving antennas. The accuracy of this calculation procedure has been shown to be in excellent agreement with measured data in Fig. 21. Since absolute gain determination is not possible without the calibration from the elevated dipole test antenna (or suitable equivalent), only a relative scale is presented with the horizontal patterns. The measured and theoretical patterns are again in good agreement.

The power received by a quarter-wave monopole at 150 MHz is plotted in Fig. 28 along with the calculated distribution (solid curve). The pattern determined for the electrode antenna for vertical polarization at $\phi = 0^\circ$ is shown in Fig. 29, and the power gain at 16° incidence is in good agreement with the value of -23 dB calculated from Eq. (7). At 130 MHz the hypothesized interference effect predicts a decrease in gain as $\theta = 90^\circ$ is approached, but the effect of maximum subtractive interference (at $g = 1$) is never achieved because g increases to a maximum of $0.91\ \lambda$ at $\theta = 90^\circ$. This prediction is supported by the observations since there is a tendency for the data to fall below the theoretical prediction for large values of θ, whereas at frequencies near 250 MHz, the data exceed the theoretical estimate.

The relative pattern for horizontal polarization at $\phi = 90^\circ$ is shown in Fig. 30 and is in good agreement with the theoretically predicted distribution.

The data from measurements at 400 MHz are shown in Figs. 31, 32, and 33. The large asymmetry in the vertical polarization pattern at $\phi = 0^\circ$ and $\phi = 180^\circ$ is shown in Fig. 32 by the solid (theoretical) curves. The power gain of -23.2 dBi indicated by the theoretical curves at $\theta = 0^\circ$ was determined by Eq. (7). Data were taken on the electrode antenna at $\phi = 180^\circ$, and agreement with the theoretical pattern is poor in the 40° to 80° region. The low value of the measured gain in this region can be explained by the interference hypothesis; however, it is necessary to assume that the antenna is displaced 11 cm from the center of the tank -- a likely possibility since no special effort was devoted to exact centering of the antenna. Using a value of $L = 0.80$ in Eq. (19), a subtractive interference maximum is predicted at $\theta = 61^\circ$ and negligible interference should occur near 90° as is observed in Fig. 32.

The data for horizontal polarization in Fig. 33 are in excellent agreement with theory as has been the case at all other frequencies.

CONCLUSIONS

A horizontal electrode antenna designed for optimum performance near 250 MHz was tested to determine its static properties of impedance, spatial patterns, power gain, and frequency response. These measurements were performed as a first step in determining the potential of this type of antenna for providing reliable reception of low data rate messages when towed near the ocean surface.

It was found that the complex impedance of the antenna can be predicted accurately by theoretical expressions previously cited in the literature, but that these expressions are complicated and are best evaluated by a computer algorithm. The impedance of the antenna at resonance is about 170 ohms and consists primarily of loss resistance, the radiation resistance being only about 0.37 ohms. Our design simulations have shown that it is difficult to reduce the loss resistance without constructing a fatter antenna.

Antenna patterns were measured for horizontal and vertical plane polarization at frequencies of 150, 250, 257.5, and 400 MHz. The patterns of the slot antenna and electrode antenna at resonance (250 MHz for electrode antenna, 255 MHz for the slot antenna) are nearly identical. Far removed from resonance the pattern of the slot antenna is inconsequential because the power gain diminishes rapidly. However, since the power gain of the electrode antenna remains appreciable over the range of frequencies indicated, pattern measurements are of interest at various frequencies in the band. Because the antenna is fed at one end, there is an asymmetry in the E_θ pattern measured in a vertical plane coinciding with the axis of the antenna. The asymmetry is small at and below resonance but produces gain differences as great as 7 dB at 400 MHz.

A comparison of the power gain of the electrode antenna with a slot antenna borrowed from MIT-LL was performed at incidence angles of 16° and 66° with respect to the vertical. The slot antenna was reported by MIT-LL to have a static gain in salt water of -9.7 dB relative to isotropic and 3 dB bandwidth of 11.5 MHz [1]. Other slot antennas have been constructed by MIT-LL with gains ranging from -2 to -12 dB relative to isotropic depending on bandwidth (3 to 11 MHz) and diameter of the flotation jacket. The particular slot antenna borrowed from them for our comparison measurements is believed to represent a good compromise in the design variables of gain, bandwidth, and diameter of the flotation jacket (4 cm).

At an incidence angle of 16° from the vertical the electrode antenna had a gain of about 8.5 dB less than the slot antenna. Accounting for an impedance mismatch with the electrode antenna, a 1.5 dB improvement is possible; therefore, the power gain of the electrode antenna will be at least 7 dB below that of the slot.

At the more shallow angle of incidence (66° from vertical) the experimental results were less definitive because of mismatch problems with the receiver (see MEASUREMENTS and RESULTS) and a suspected interference problem from reflections at the edge of the salt water test tank. In brief, the power gain of the electrode antenna was not improved relative to that of the slot antenna, and no improvement is expected theoretically.

A semi-analytical method of computing the frequency response and magnitude of the power gain of the electrode antenna using calculated parameters or a mixture of calculated and measured parameters was outlined. At an incidence angle of 16° from the vertical, the calculated power gain agreed well in magnitude and frequency response with that measured. At an incidence angle of 66° the agreement was notably poorer because of the aforementioned mismatch problems with the receiver and a suspected interference from reflections produced at the edge of the salt water test tank.

The primary advantage of the electrode antenna for towed antenna applications is its wide frequency bandwidth. At high angles of incidence, appropriate to satellite coverage, the 3 dB passband of the antenna constructed for this study extends from 220 to 360 MHz, greater than ten times the bandwidth achievable with a slot antenna. The primary disadvantage is its low power gain, at least 7 dB lower than that of the slot antenna tested.

The quality of performance of the electrode antenna for receiving communication messages when towed near the ocean surface cannot be predicted accurately on the basis of static measurements alone. The prediction of the performance of a communications system with a towed antenna can be estimated only if dynamic gain characteristics (average and standard deviation of the statistical gain distribution) are determined for various towing speeds and sea states. The dynamic gain characteristics of the electrode antenna must be determined by monitoring the power received from the antenna while being towed in an ocean environment under carefully controlled conditions of aspect (distance and angle) between the transmitting and receiving antennas. Towing experiments of this nature have not been conducted on the electrode antenna but would represent the next logical phase of research.

The analytical concepts employed for determining the performance of an antenna having significant gain fluctuations as a consequence of its motion have been documented in [17, in which are estimated the performance of several slot antennas for receiving satellite communications with a repeated message format at 75 bits per second.

Our extrapolation of the results cited in [1] indicate that the ability of a slot antenna to receive a 150 to 300 bit communications message with 95% confidence at a rate of tenths of bits per second with a towing speed of 10 knots or greater is marginal. Since the electrode antenna has a static gain at least 7 dB lower than a typical slot antenna, its dynamic characteristics would have to be much improved over the slot antenna (high average gain relative to static, small standard deviation) in order to approach comparable dynamical performance. Consequently, unless wideband reception is required, it is doubtful that the electrode antenna should be considered as a comparable alternative to the slot antenna.

REFERENCES

1. J. C. Lee and L. S. Metzger, "Design, Test and Performance of a UHF Floating Slender-Slot Antenna," Massachusetts Institute of Technology, Lincoln Laboratories Technical Note 1977-35, December 1977.

2. J. C. Lee, "A Slender Resonator-Slot UHF Antenna Capable of Integration into a Submarine-Towed Cable," Massachusettes Institute of Technology, Lincoln Laboratories Technical Note 1976-5, January 1976.

3. E. H. Flath, Jr. and O. Norgorden, "Expressions for the Input Impedance and Power Dissapation in Lossy Concentric Lines," NRL Report R-3436, 24 March 1949.

4. C. T. Fessenden and D. H. S. Cheng, "Development of a Trailing-Wire E-Field Submarine Antenna for Extremely Low Frequency (ELF) Reception," IEEE Transactions on Communications, Vol. Com-22, No. 4, pp. 428-437, April 1974.

5. R. C. Fenwick and W. L. Weeks, "Submerged Antenna Characteristics," IEEE Trans. Antennas Propagat., AP-11, p. 296, May 1963.

6. A. W. Biggs, "Radiation Fields from a Horizontal Electric Dipole in a Semi-Infinite Conducting Medium," IRE Trans. Antennas Propagat., AP-10, pp. 358-362, July 1962.

7. A. W. Biggs and H. M. Swarm, "Radiation Fields of an Inclined Electric Dipole Immersed in a Semi-Infinite Conducting Medium," IEE Trans. Antennas Propagat., AP-11, pp. 306-310, May 1963.

8. E. C. Jordan and K. G. Balmain, Electromagnetic Waves and Radiating Systems, Second Edition, Prentice-Hall, Inc., Englewood Cliffs, NJ, p. 235, 1968.

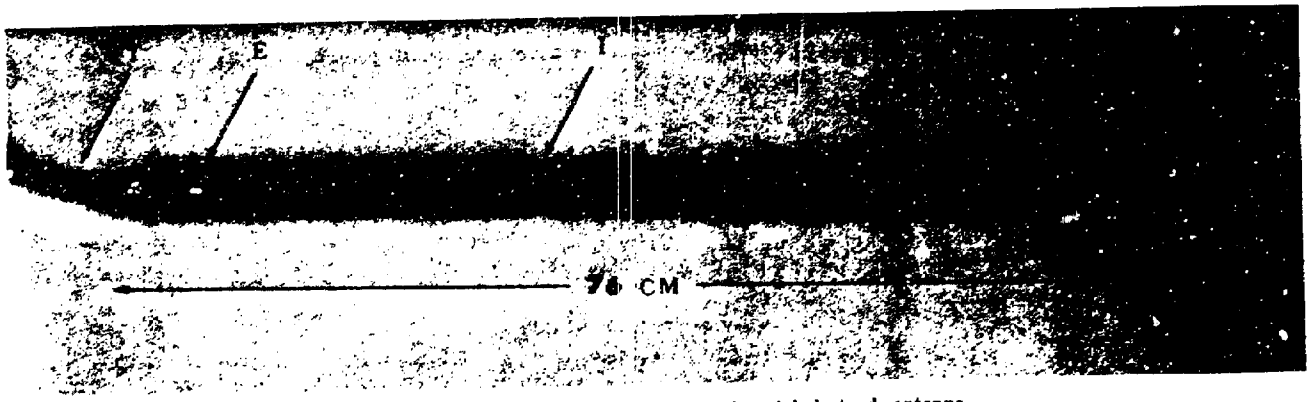

Fig. 1 — External appearance of the experimental electrode antenna

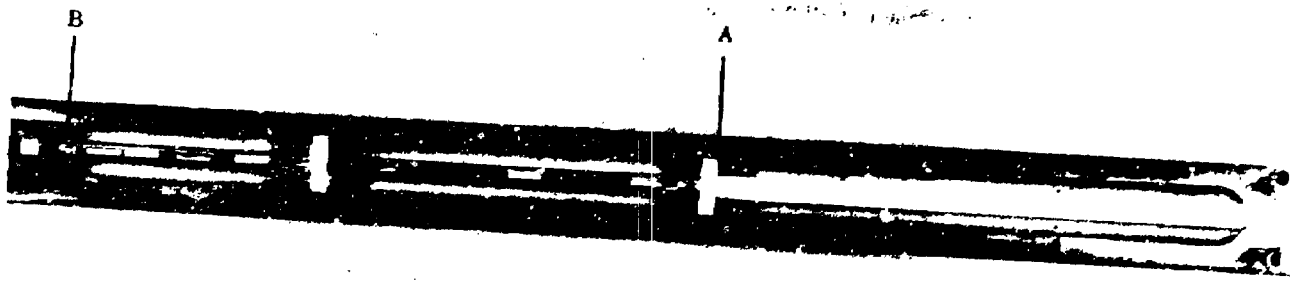

Fig. 2 — Overhead view of the internal components of the electrode antenna mounted in one half of the aluminum mold used for casting the outer insulating jacket

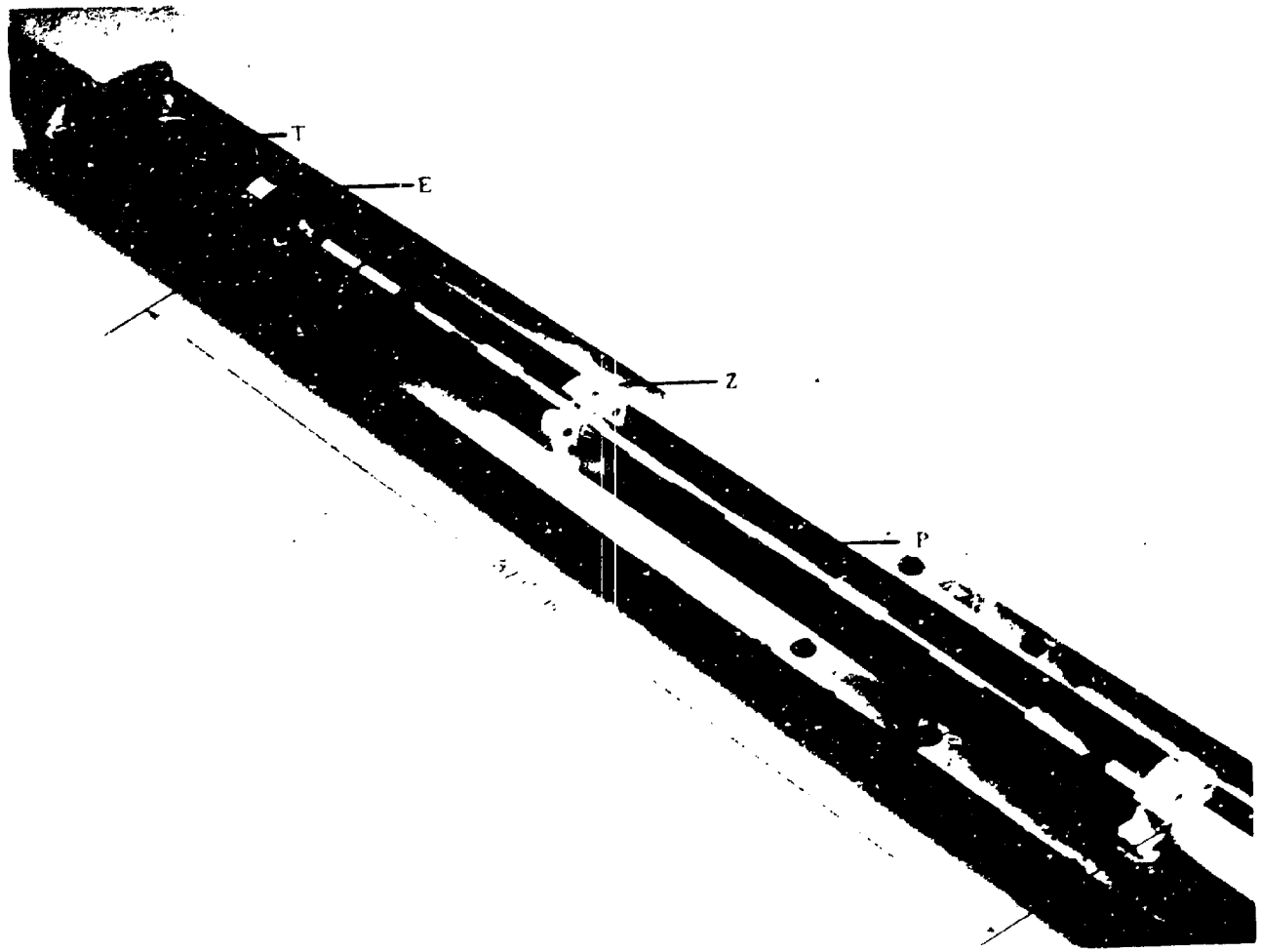

Fig. 3 – Skewed view of the internal components of the electrode antenna

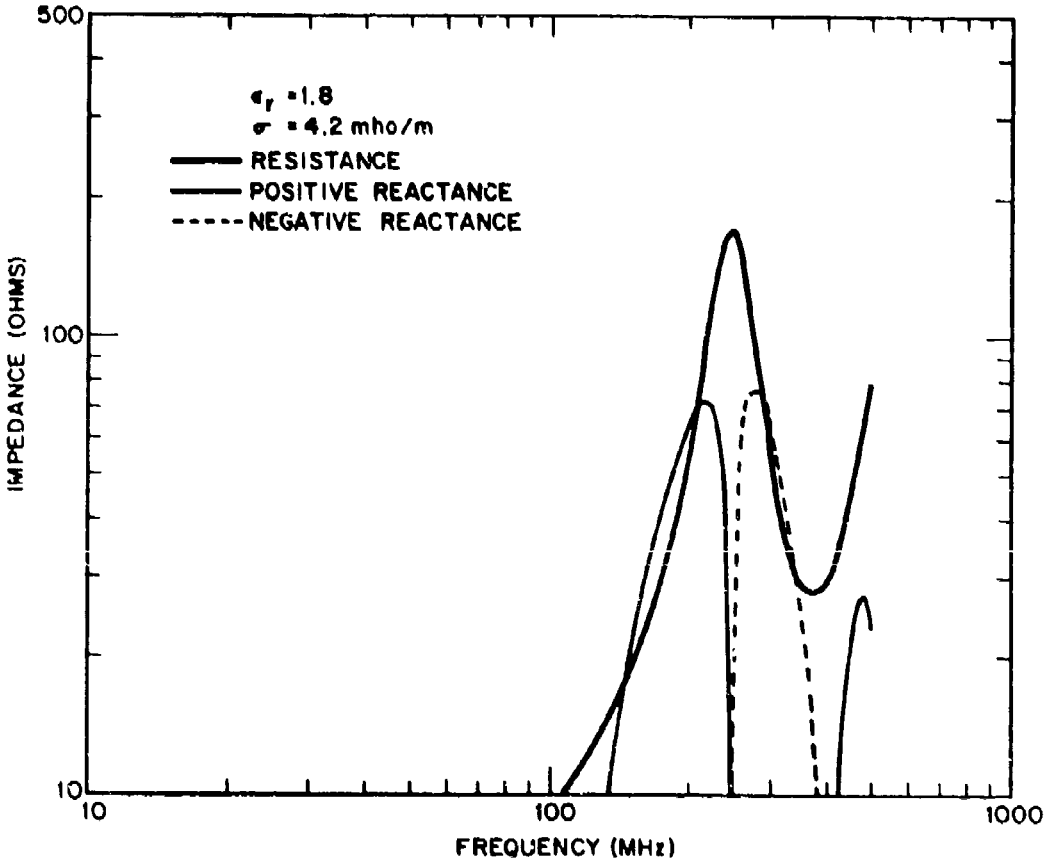

Fig. 4 — Calculated impedance of the electrode antenna

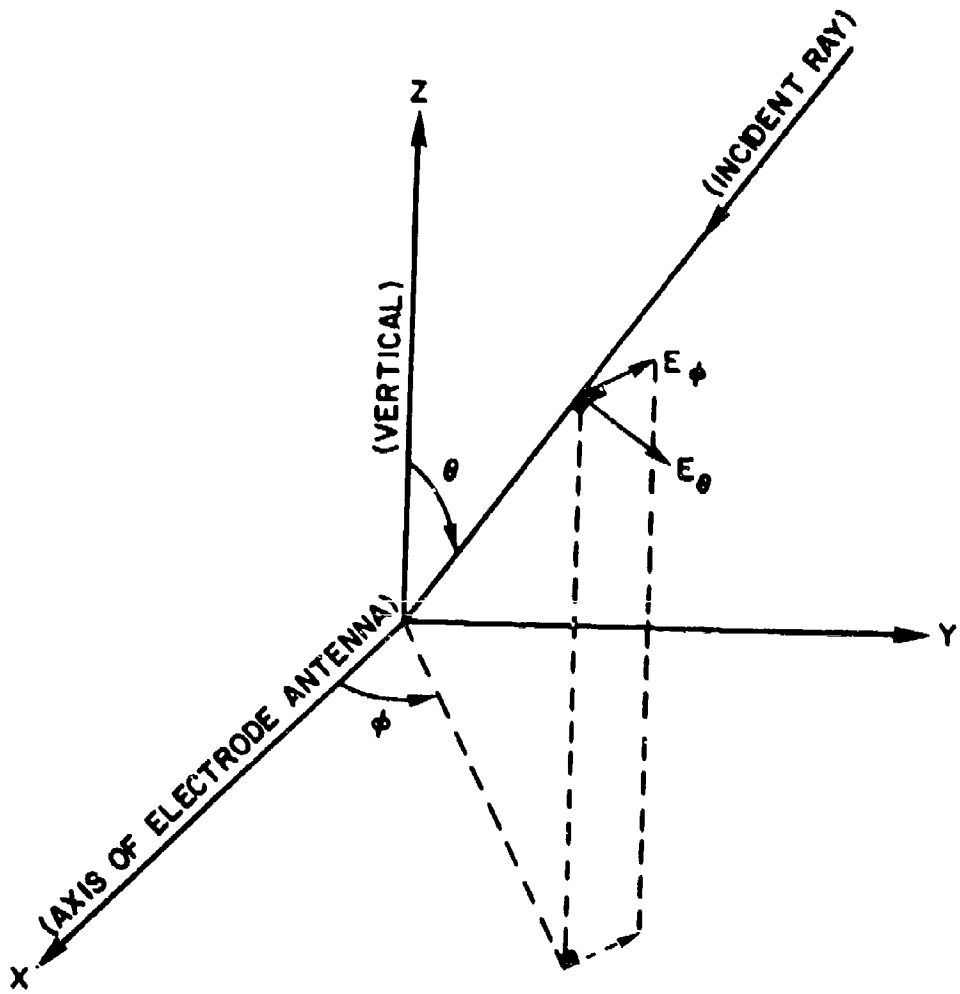

Fig. 5 — Relationship of coordinate system, antenna axis, and E_θ, E_ϕ field components

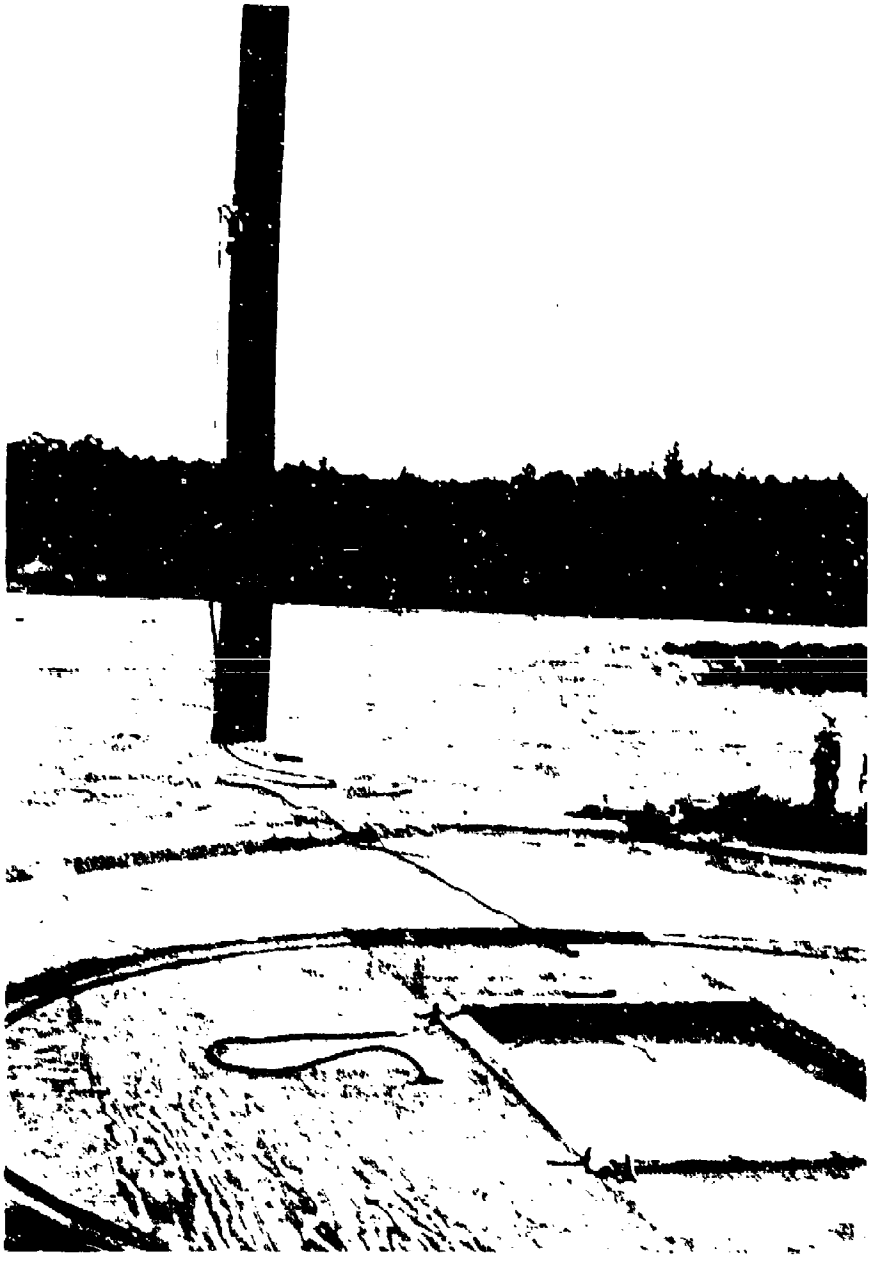

Fig. 6 — Experimental setup for determination of power gain and frequency response for the electrode antenna with polarization in the vertical plane

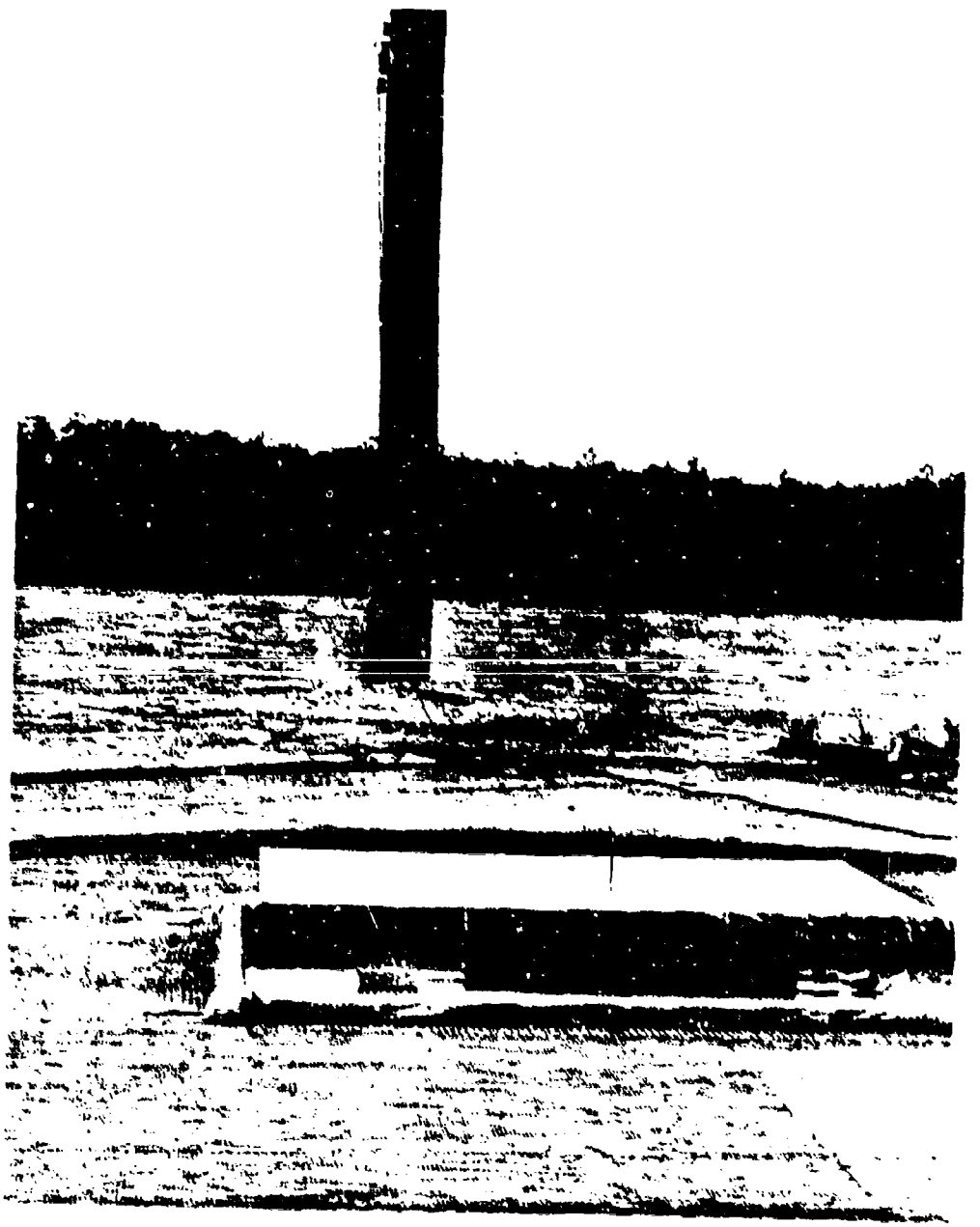

Fig. 7 – Experimental setup for calibration of transmitting dipole and for determination of power gain and frequency response for the slot antenna with polarization in the vertical plane

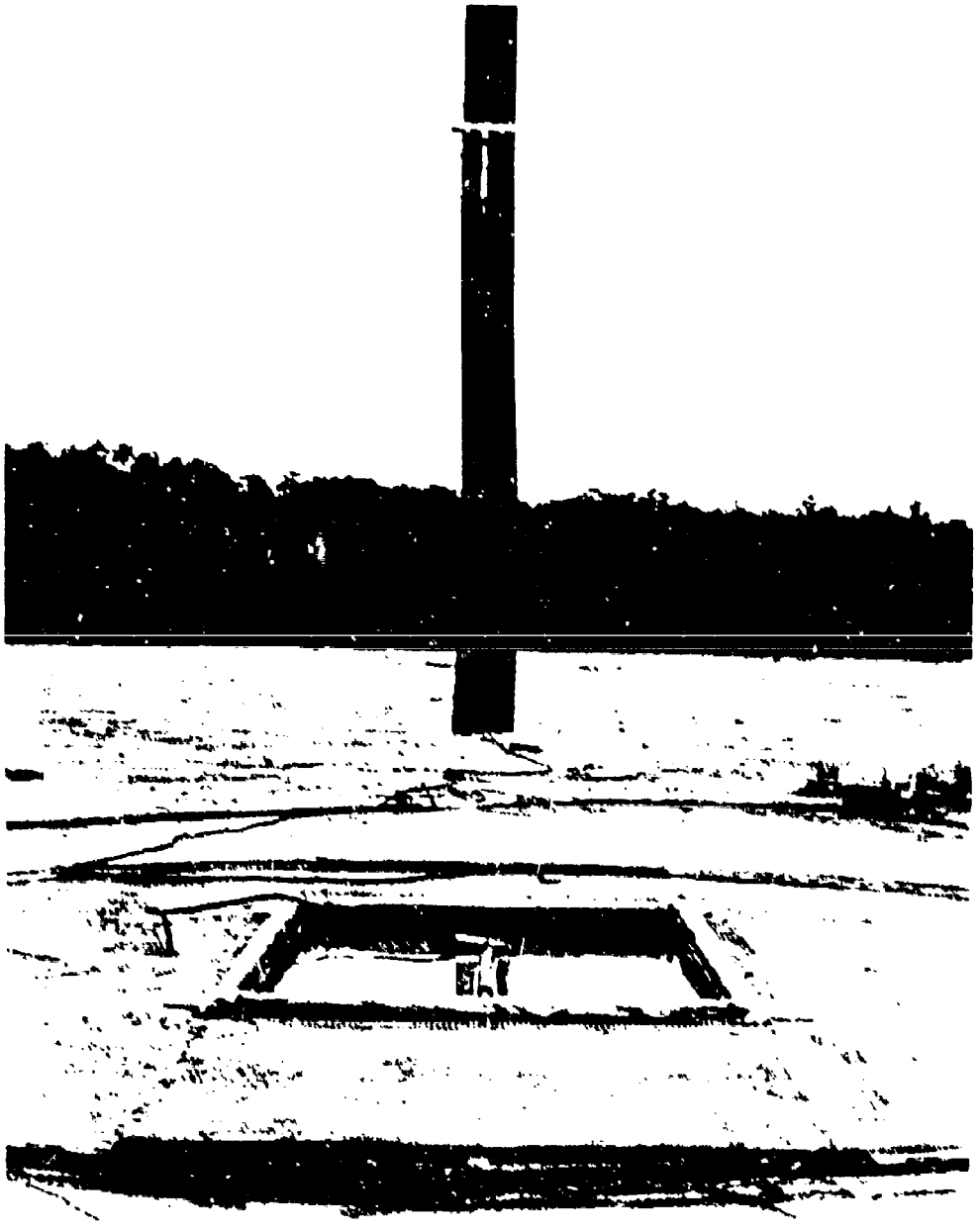

Fig. 8 Experimental setup for determination of power gain and frequency response for the slot antenna with polarization in the horizontal plane

Fig. 9 — Experimental set-up for measurements with horizontal polarization at near vertical incidence ($\theta = 16^{\circ}$)

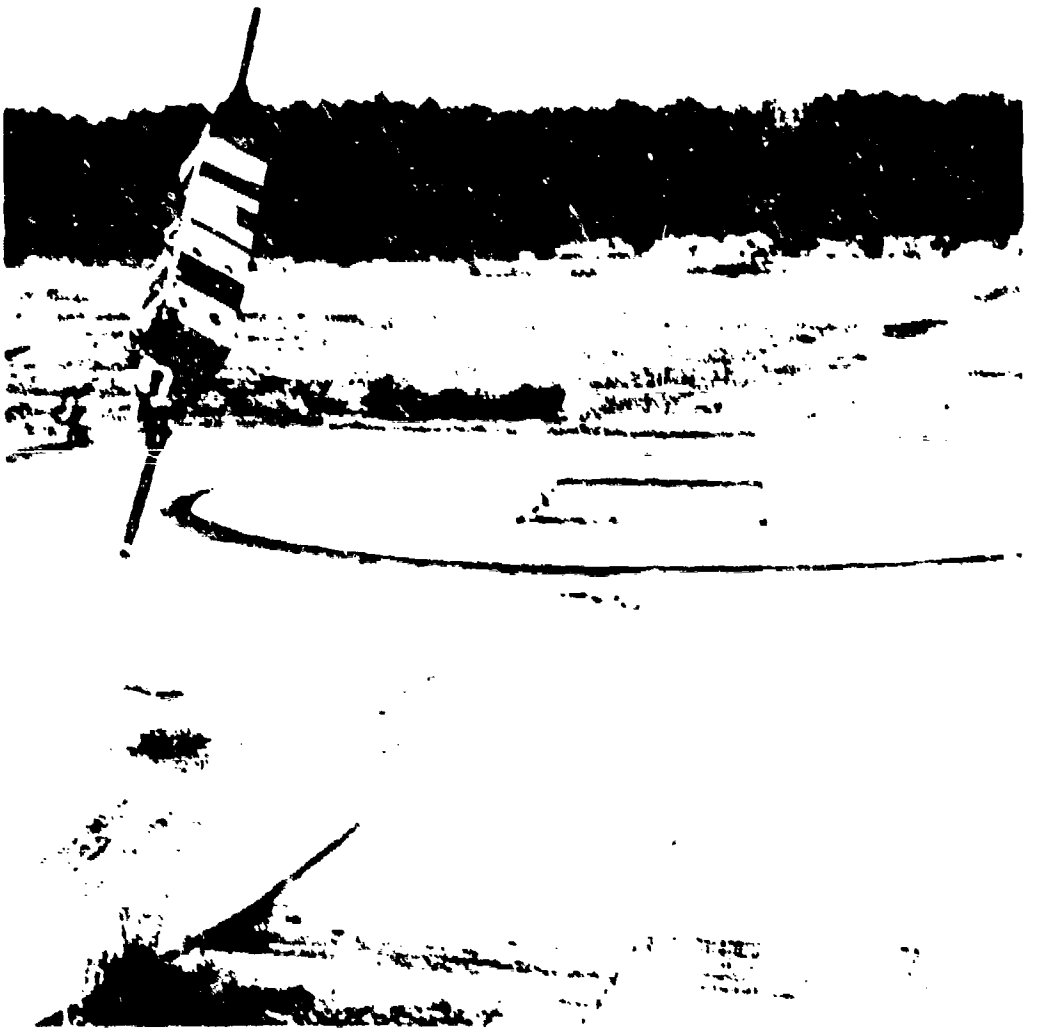

Fig. 10 — Experimental setup for measurement of spatial patterns with polarization in the vertical plane

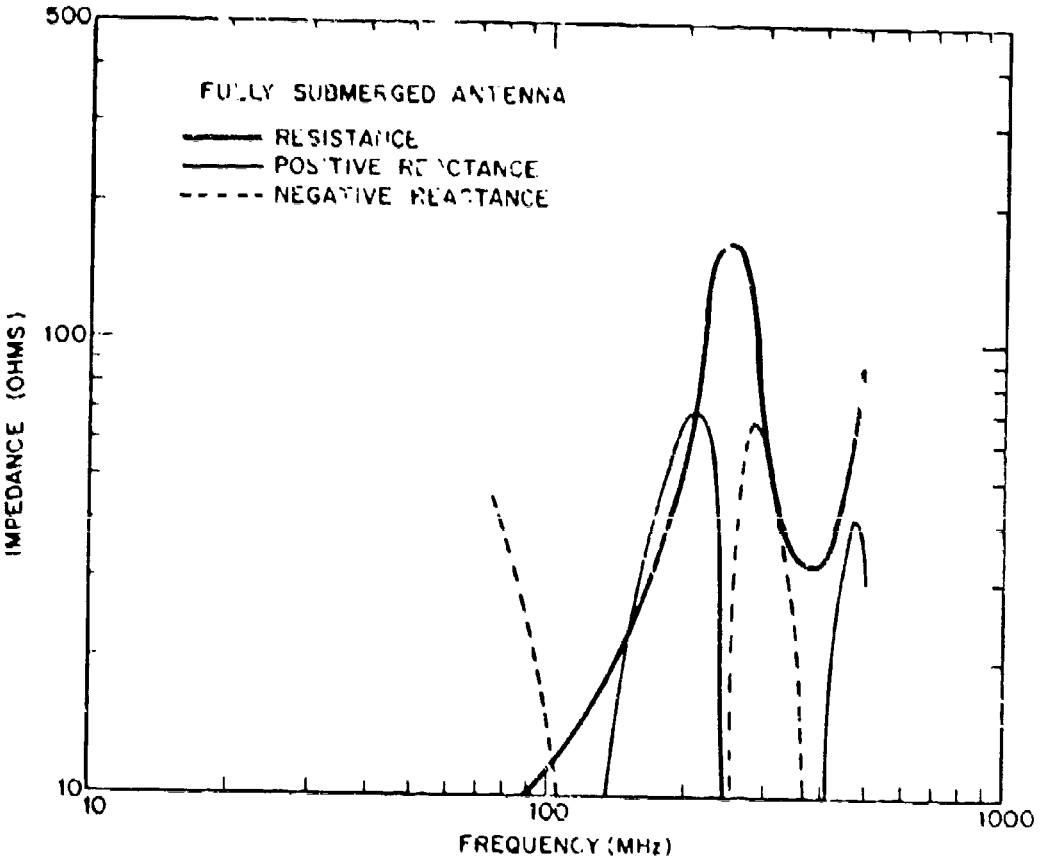

Fig. 11 — Measured impedance of the electrode antenna (fully submerged in salt water)

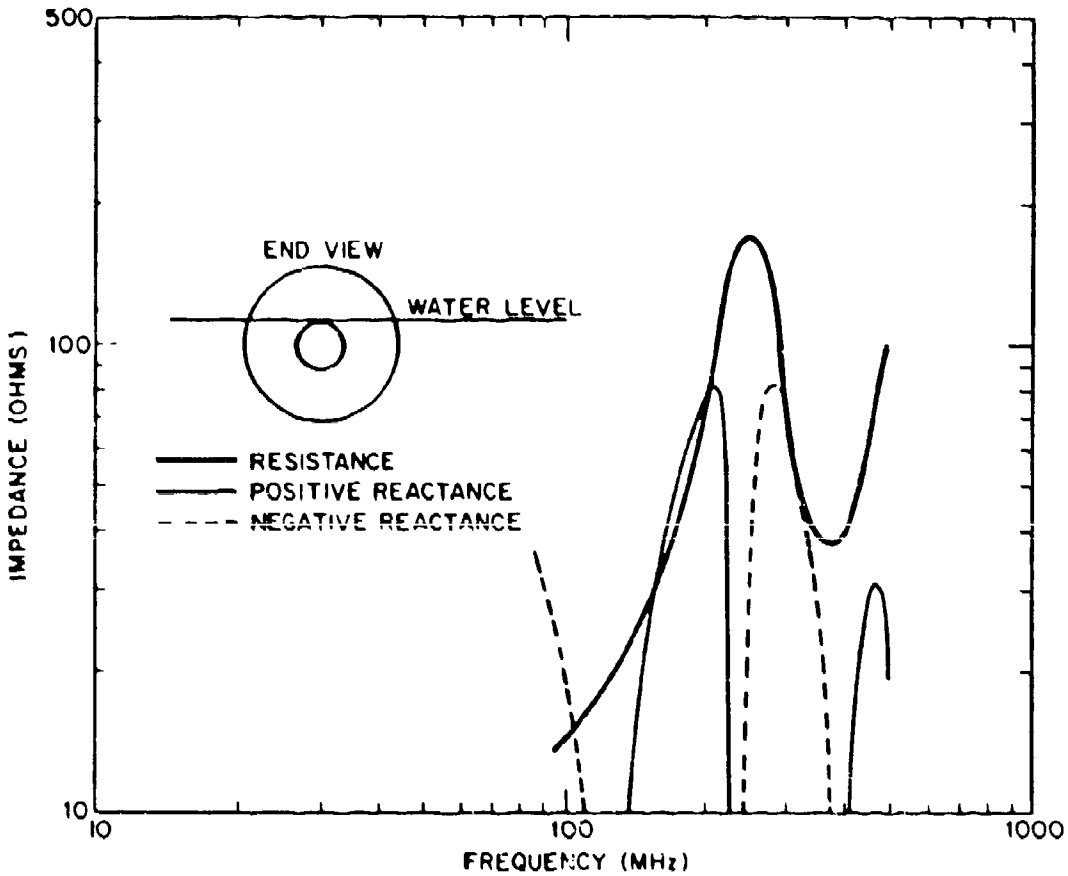

Fig. 12 – Measured impedance of the electrode antenna (cross-section 3/5 submerged)

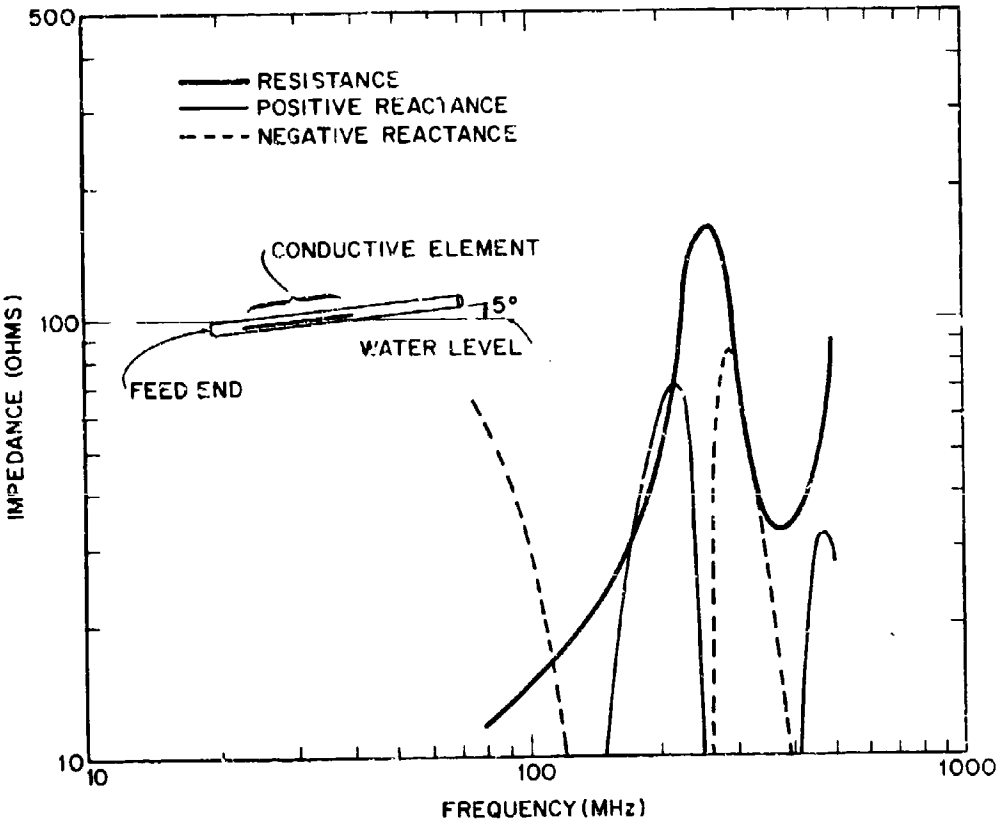

Fig. 13 — Measured impedance of the electrode antenna (tipped 5 degrees)

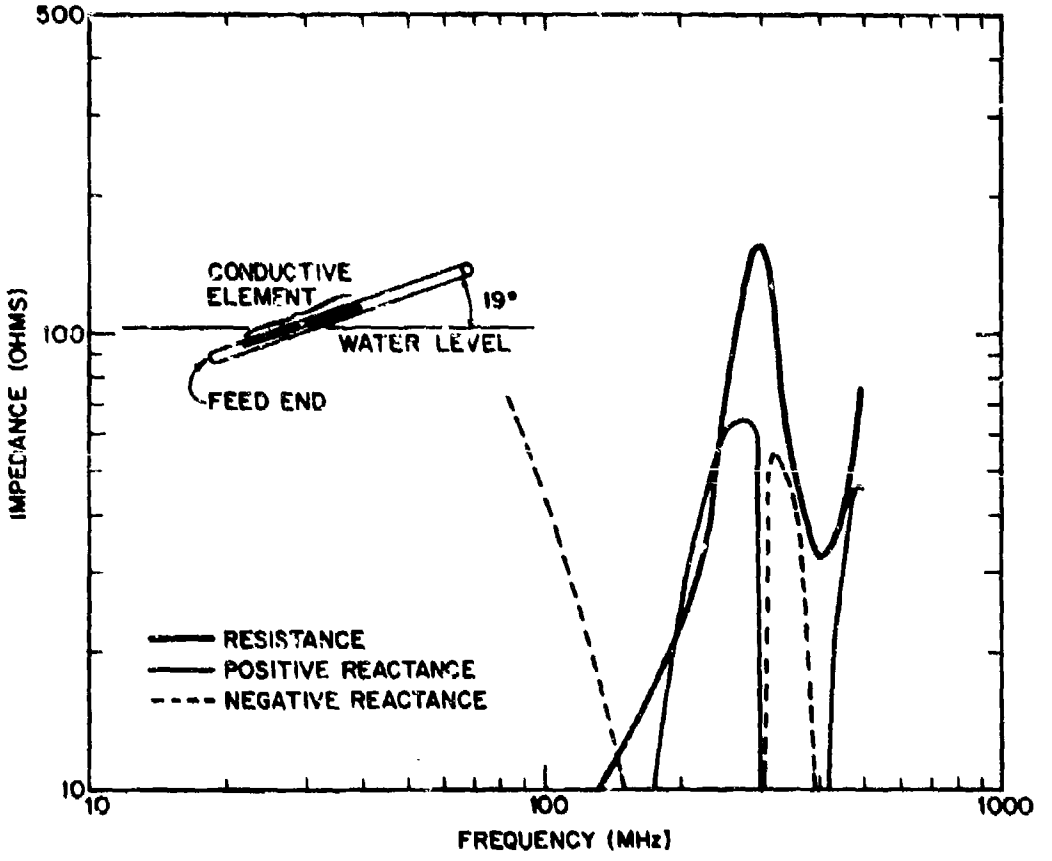

Fig. 14 — Measured impedance of the electrode antenna (tipped 19 degrees)

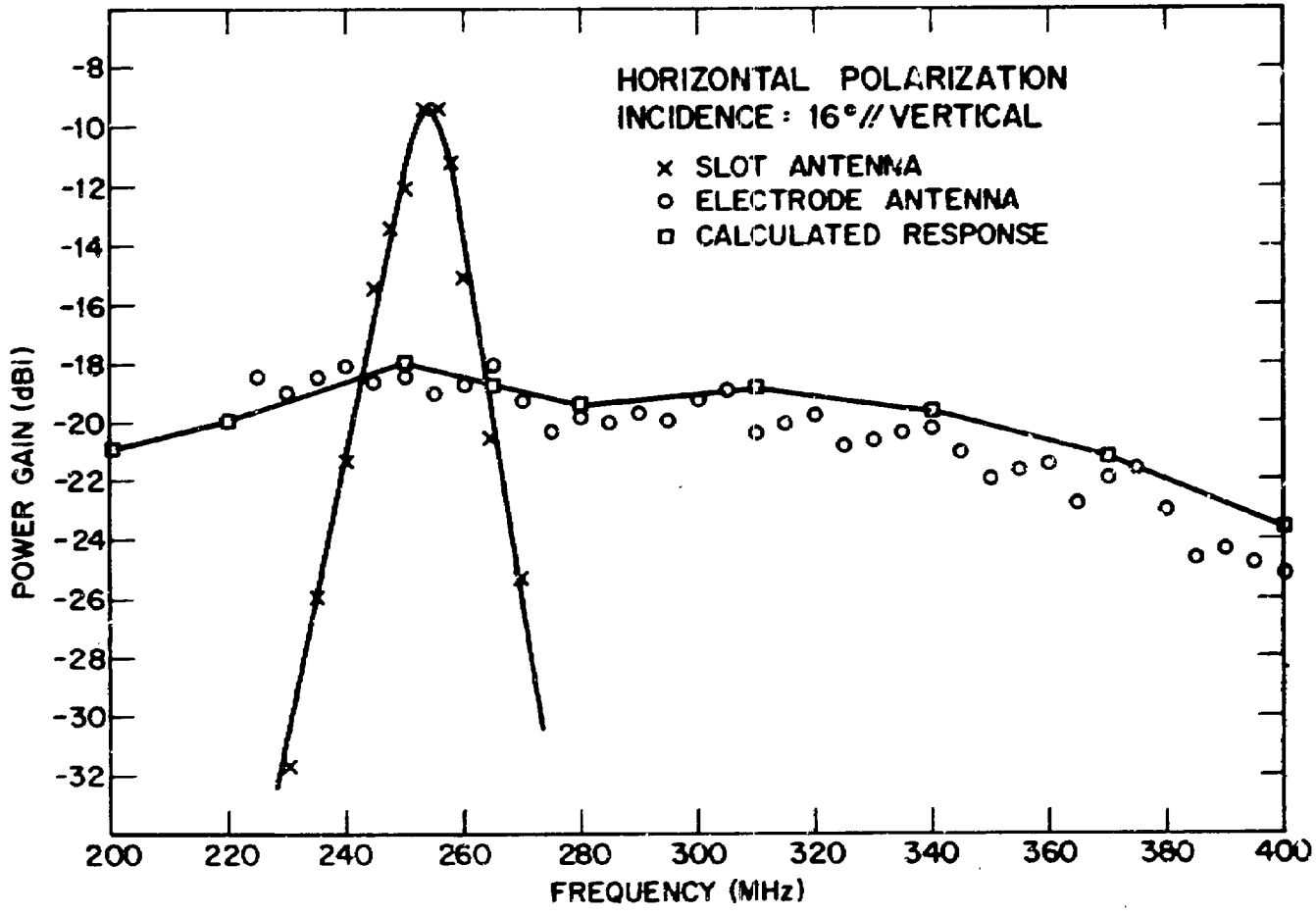

Fig. 15 — Frequency response and magnitude of the power gain for the electrode and slot antennas for horizontal polarization at an incidence angle of 16° from vertical

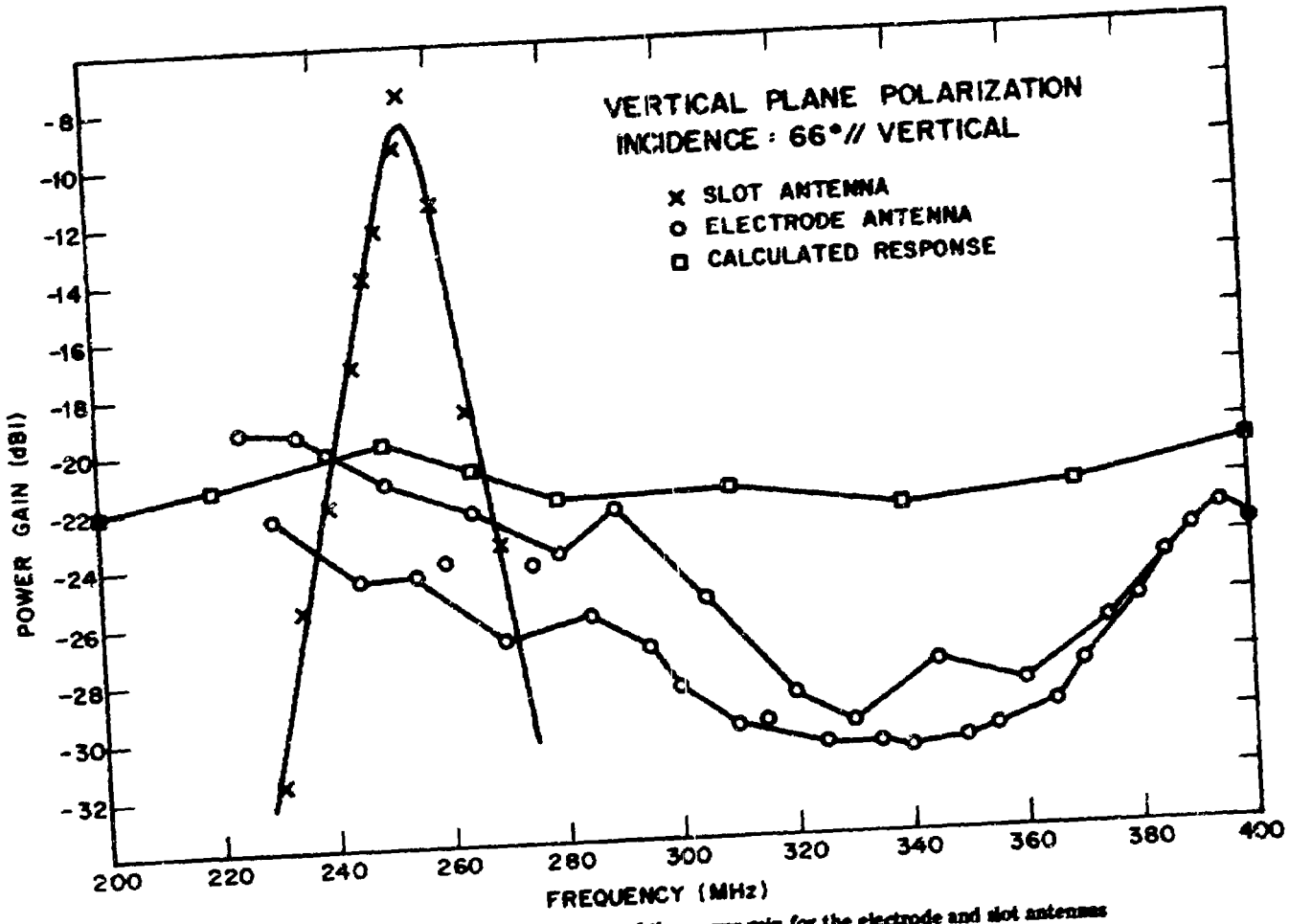

Fig. 16 — Frequency response and magnitude of the power gain for the electrode and slot antennas for vertical polarization at an incidence angle of 66° from vertical

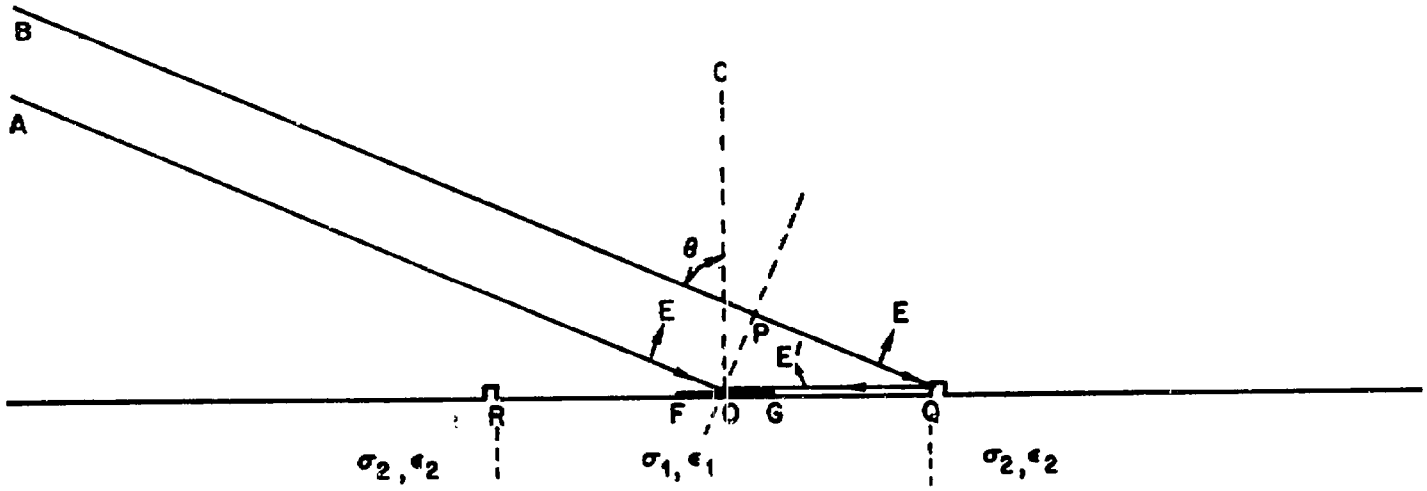

Fig. 17 — Model showing interference of direct ray to the antenna with a secondary ray reflected at the edge of the test tank

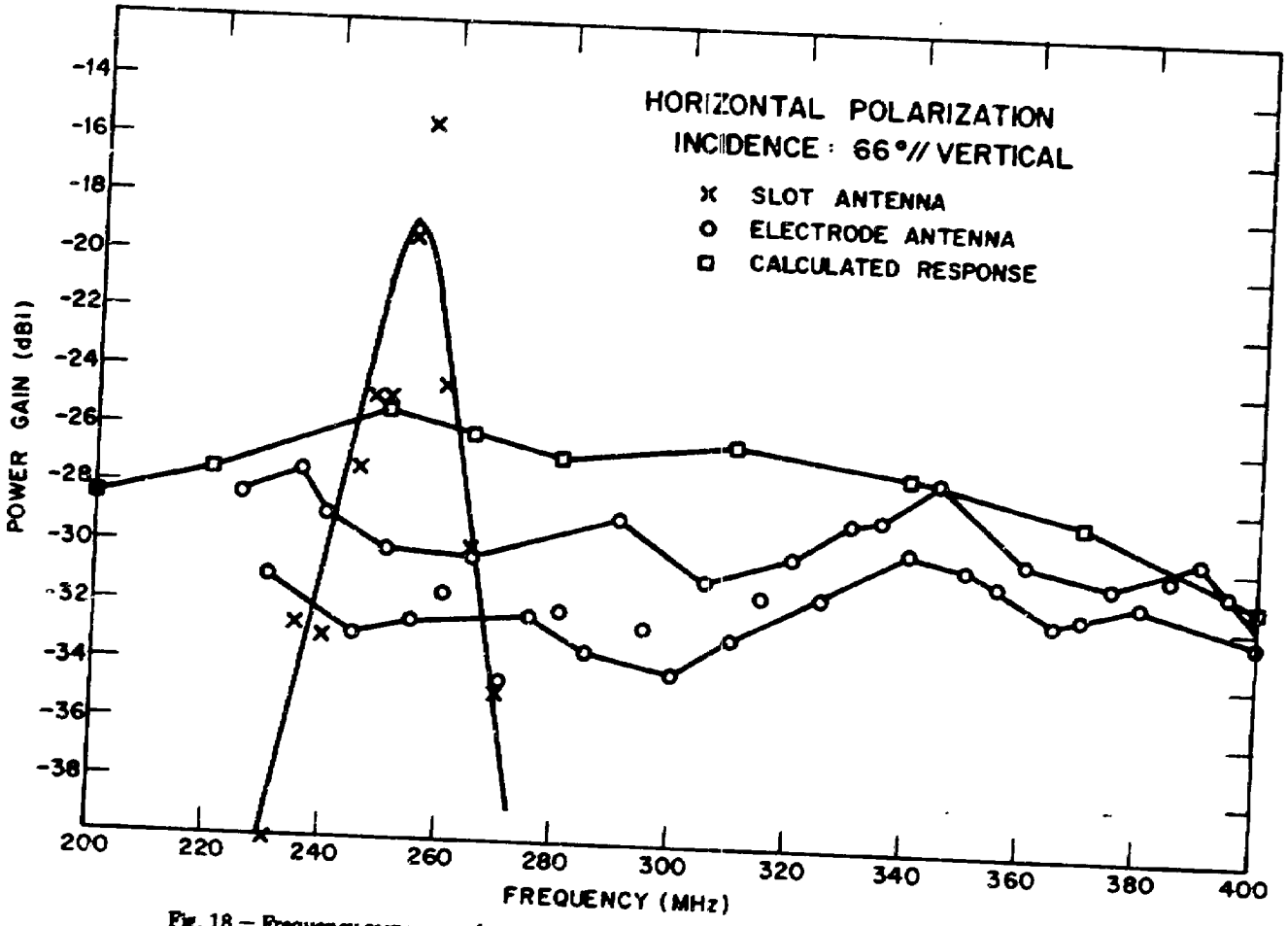

Fig. 18 — Frequency response and magnitude of the power gain for the electrode and slot antennas for horizontal polarization at an incidence angle of 66° from vertical

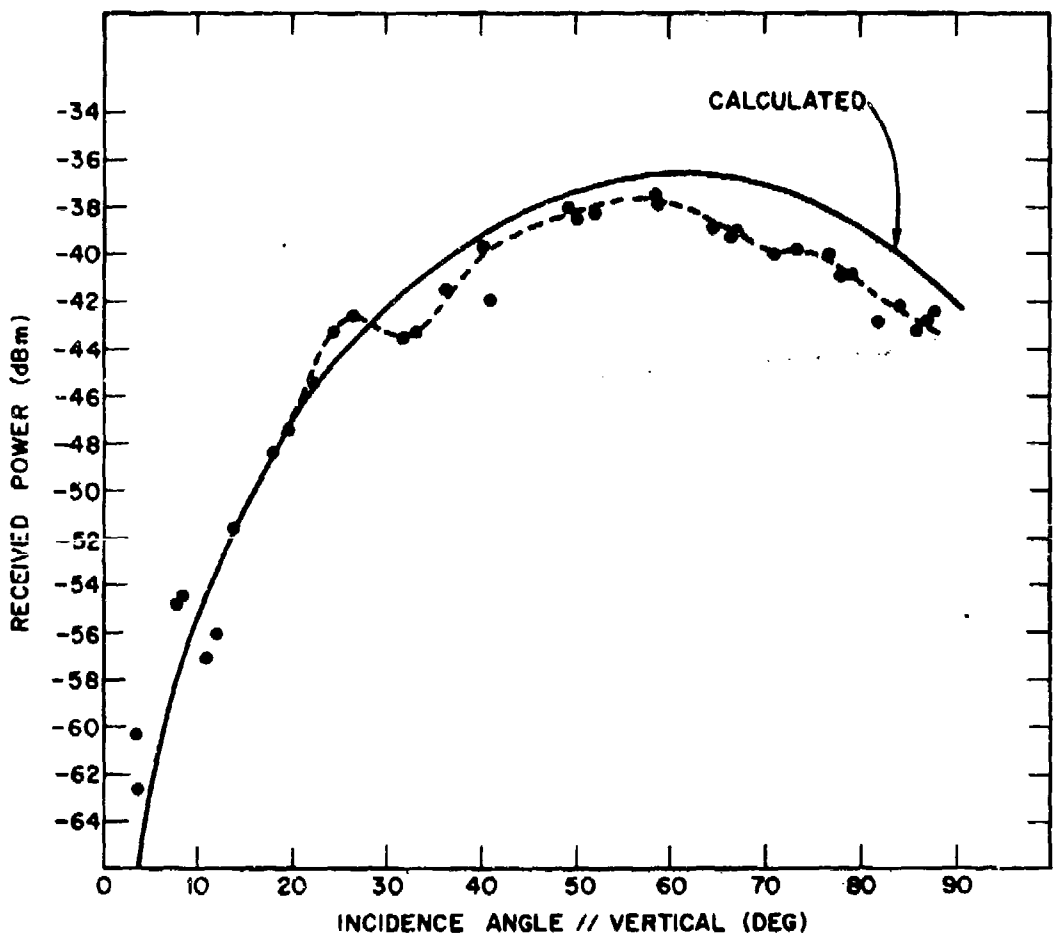

Fig. 19 — Calculated and measured monopole response at 257.5 MHz

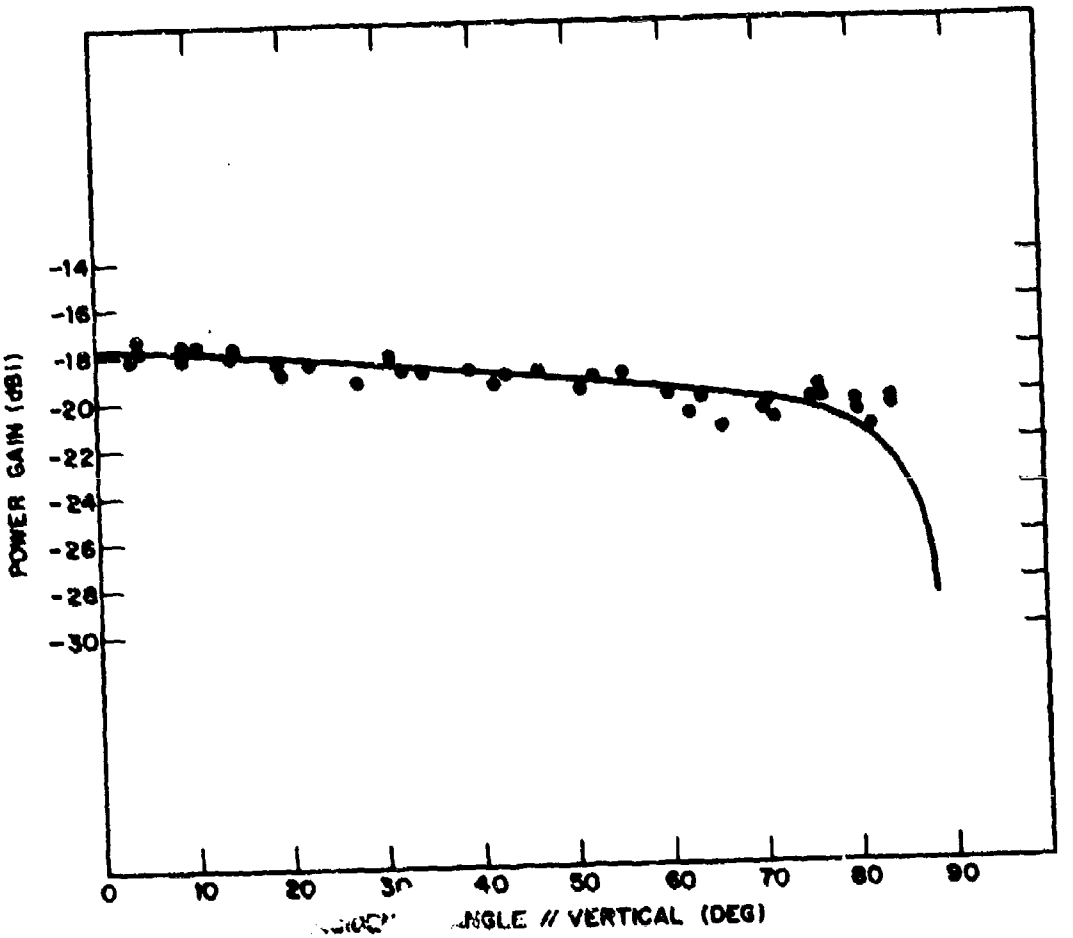

Fig. 20 — E_θ pattern for electrode antenna at 257.6 MHz (along antenna axis, vertical plane polarization)

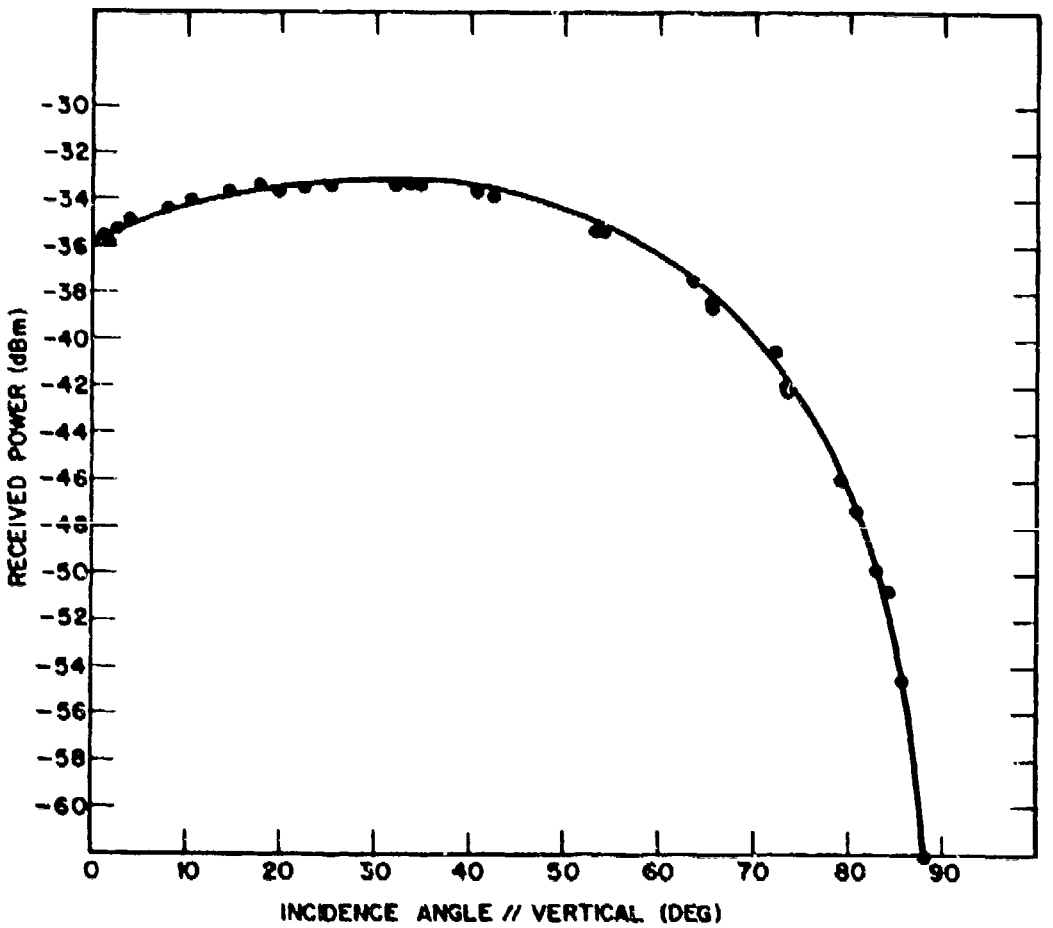

Fig. 21 — Calculated and measured response of a dipole antenna mounted 0.23 wavelengths above a ground plane at 257.5 MHz

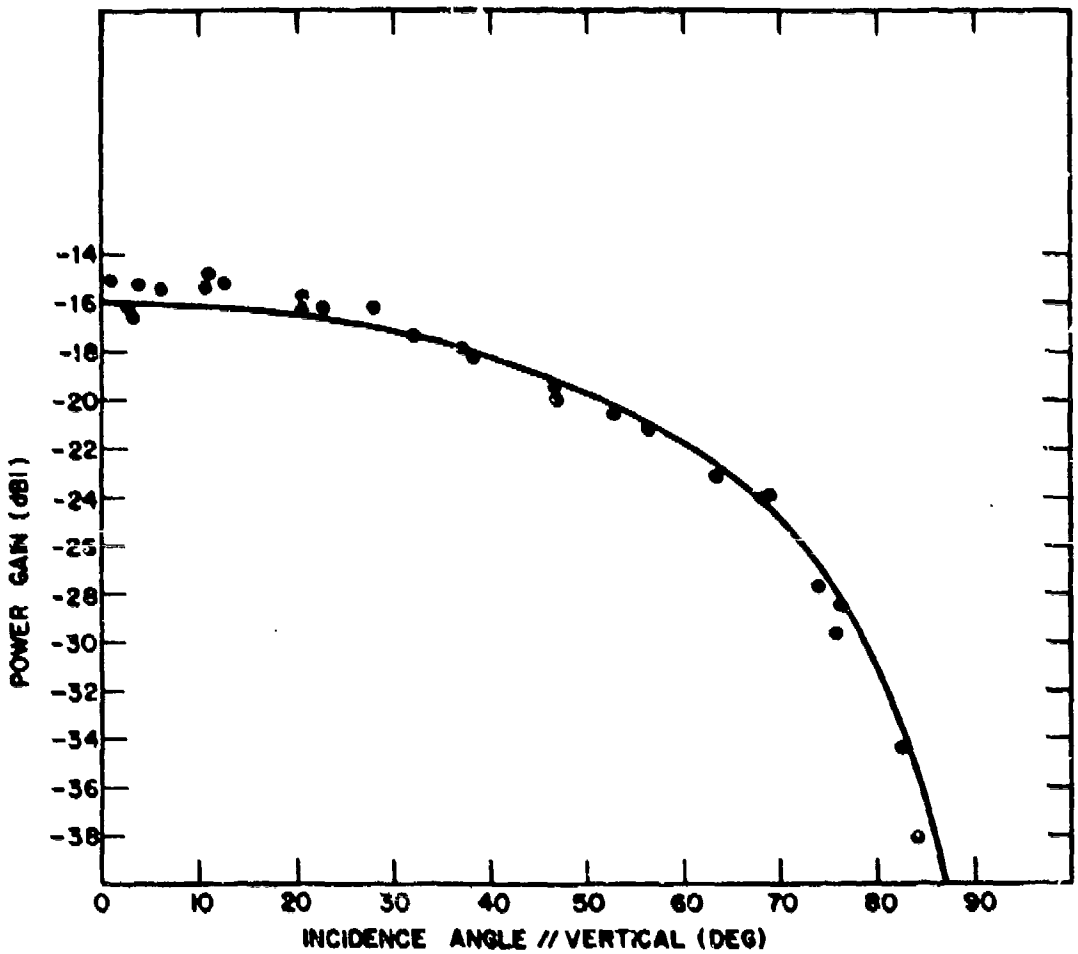

Fig. 22 — E_ϕ pattern for electrode antenna at 257.5 MHz (90° from antenna axis, horizontal polarization)

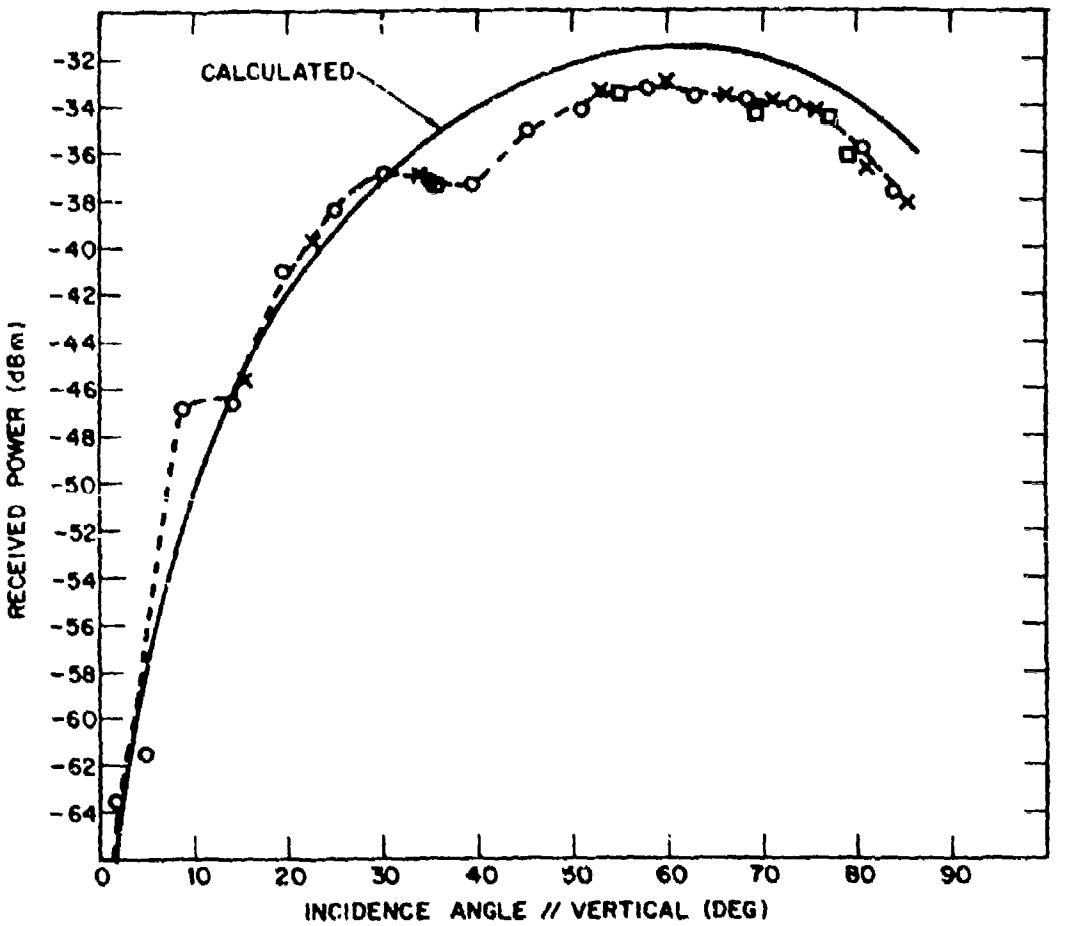

Fig. 23 — Calculated and measured monopole response at 250 MHz

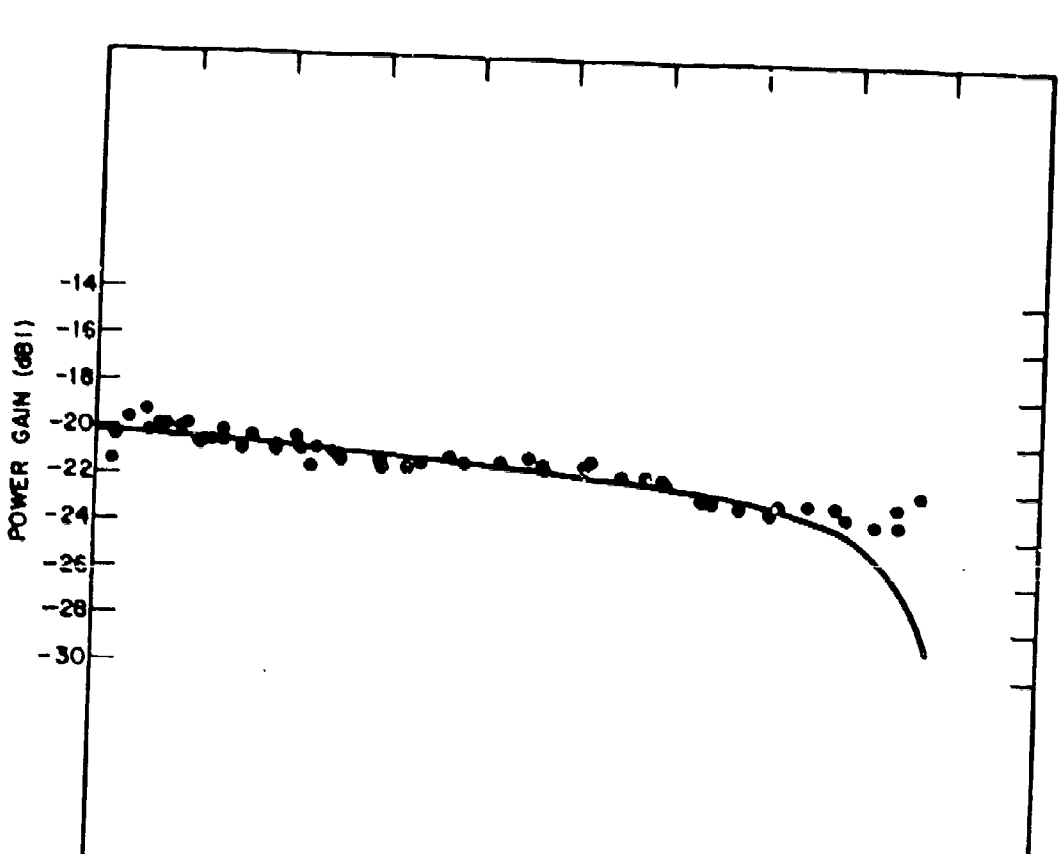

Fig. 24 – E_θ pattern for electrode antenna at 250 MHz (along antenna axis, vertical plane polarization)

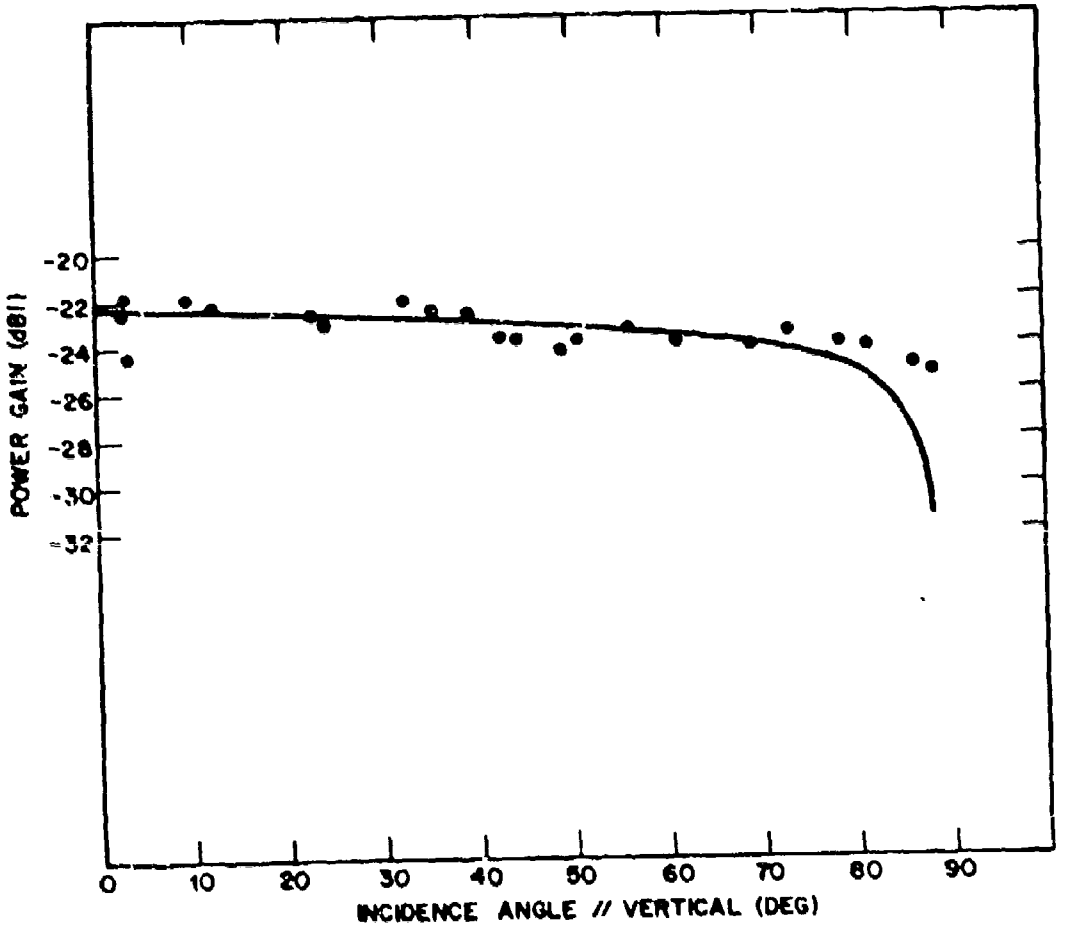

Fig. 25 – E_θ pattern for electrode antenna at 250 MHz (45° from antenna axis, vertical plane polarization)

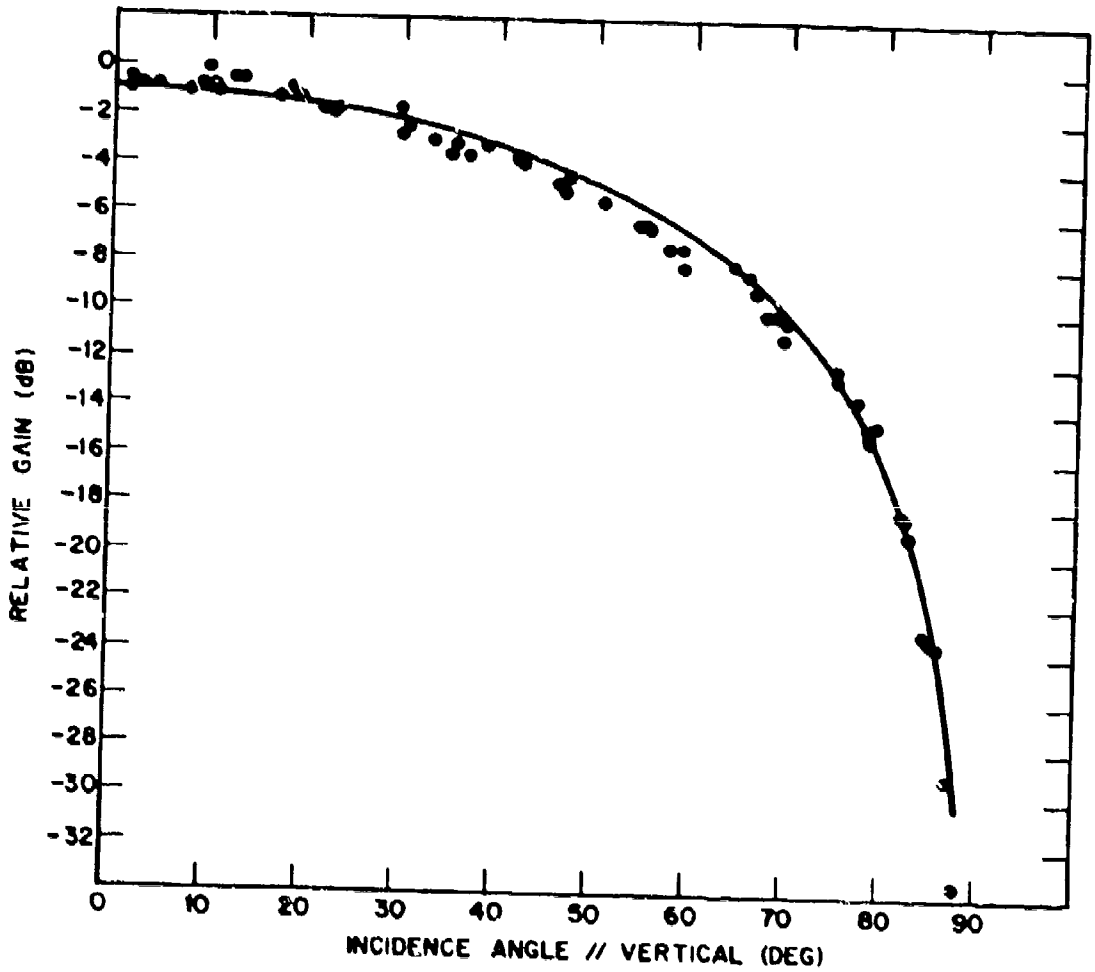

Fig. 26 – E_ϕ pattern for electrode antenna at 250 MHz (90° from antenna axis, horizontal polarization)

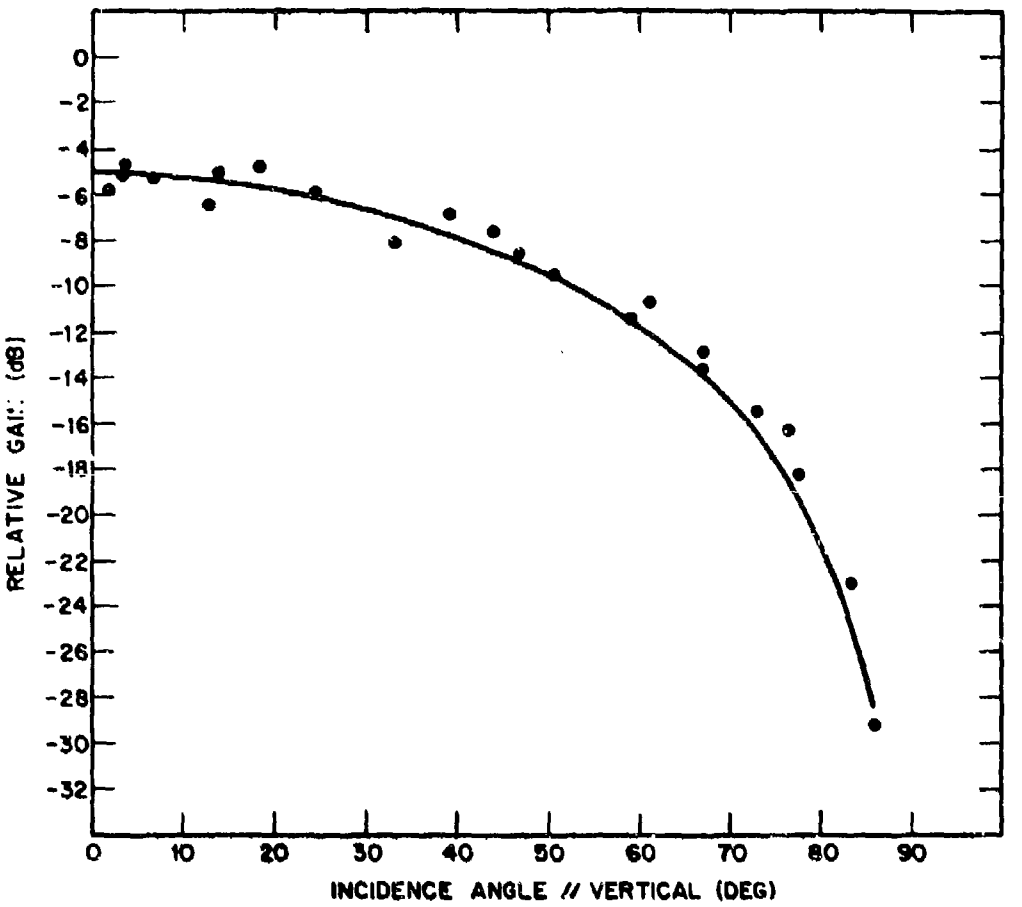

Fig. 27 — E_ϕ pattern for electrode antenna at 250 MHz (45° from antenna axis, horizontal polarization)

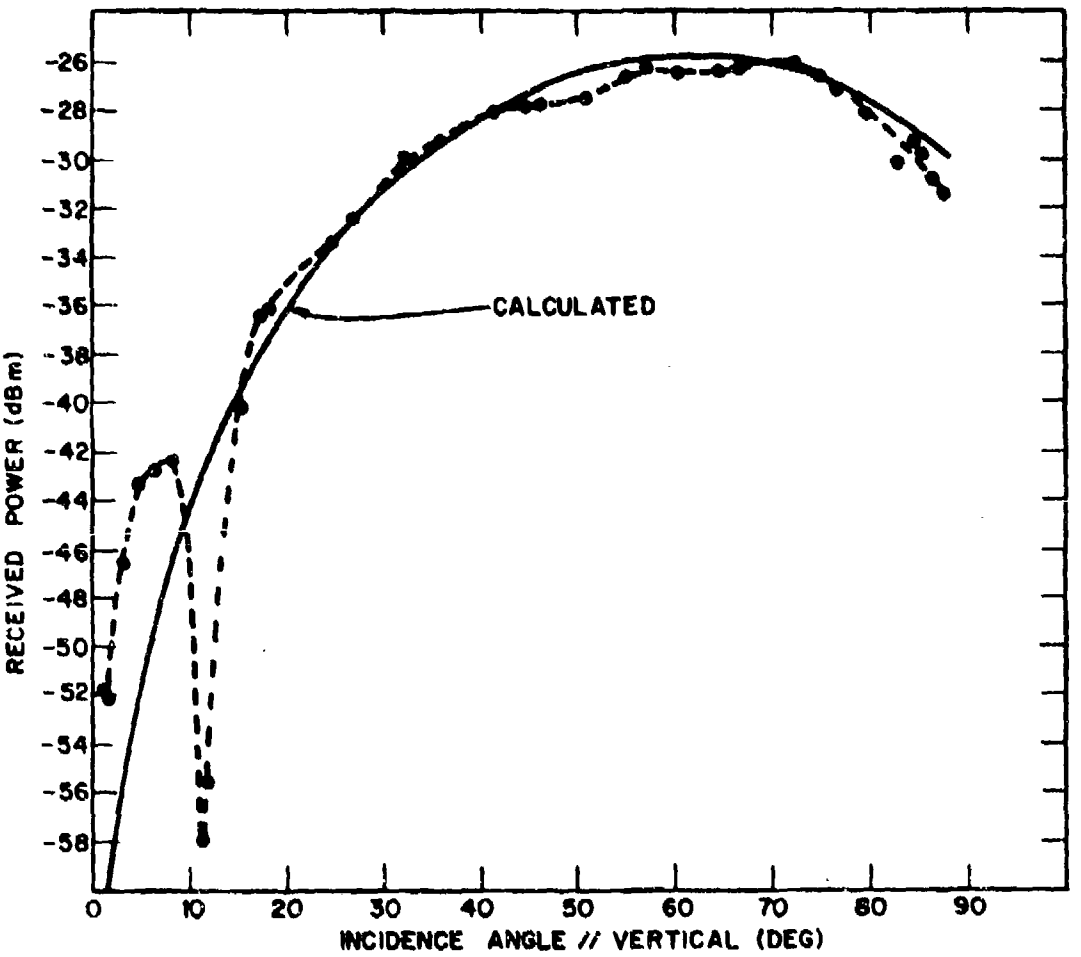

Fig. 28 — Calculated and measured monopole response at 150 MHz

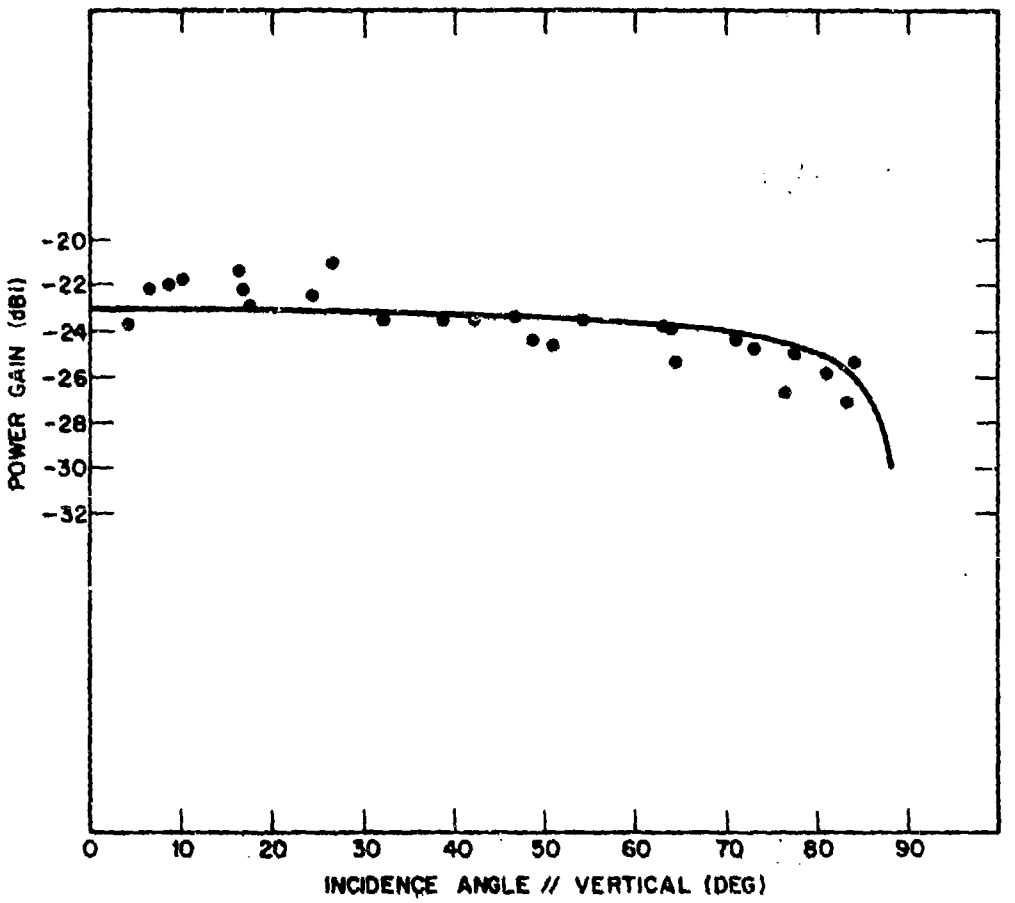

Fig. 29 — E_θ pattern for electrode antenna at 150 MHz (along antenna axis, vertical plane polarization)

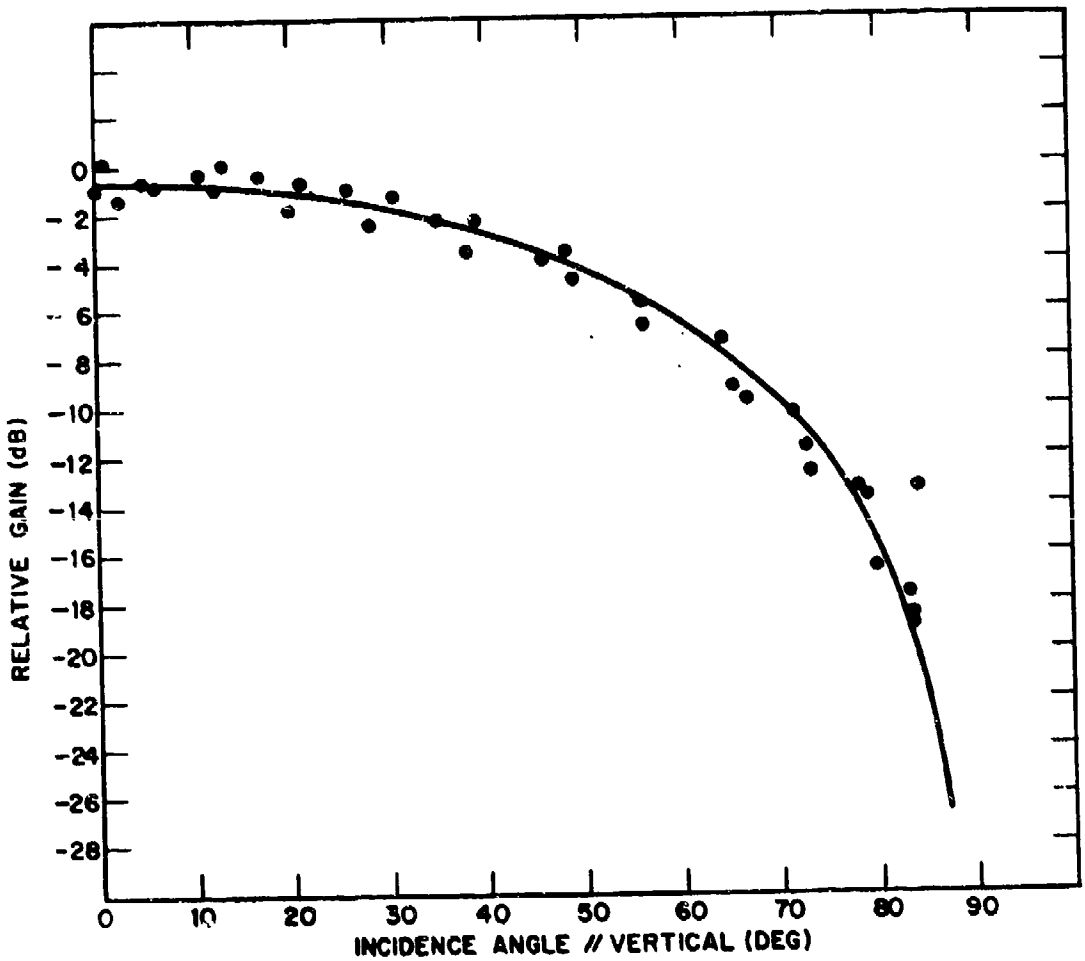

Fig. 30 — E_ϕ pattern for electrode antenna at 150 MHz (90° from antenna axis, horizontal polarization)

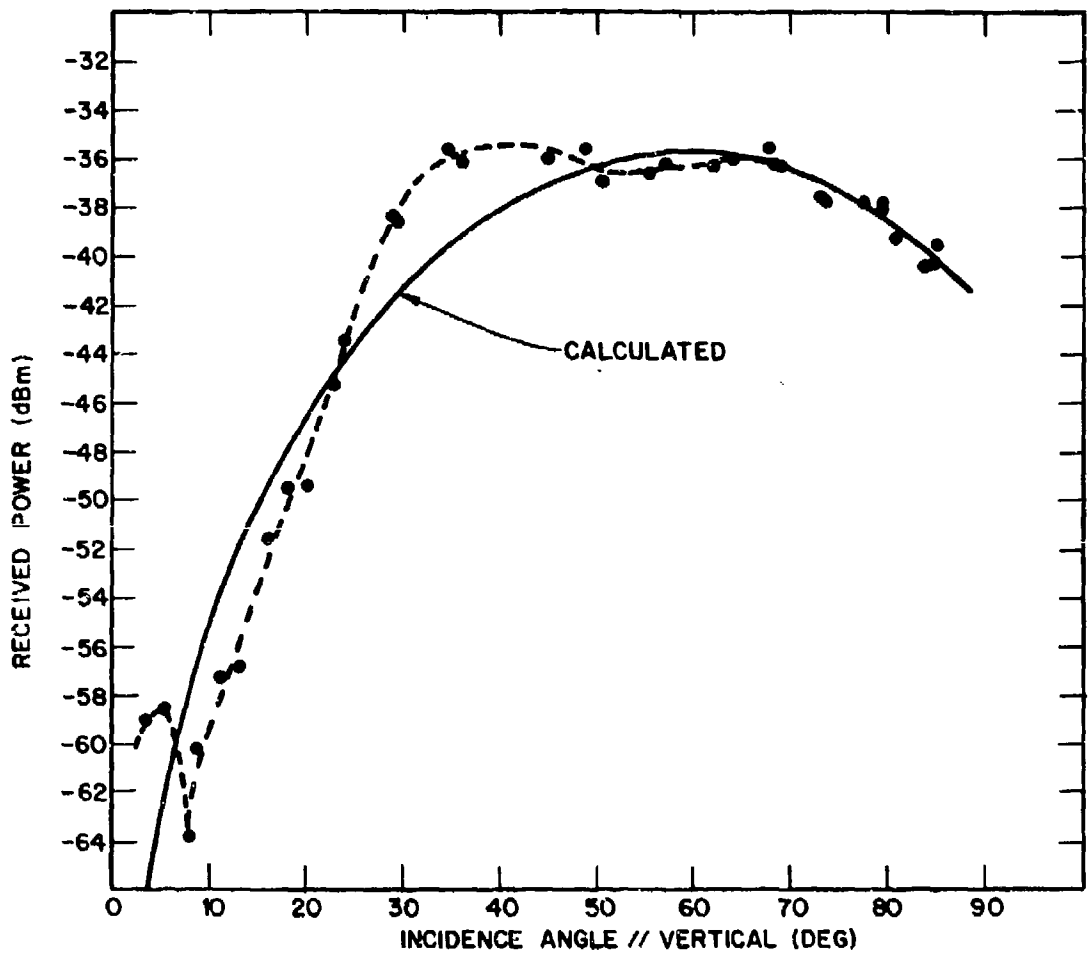

Fig. 31 — Calculated and measured monopole response at 400 MHz

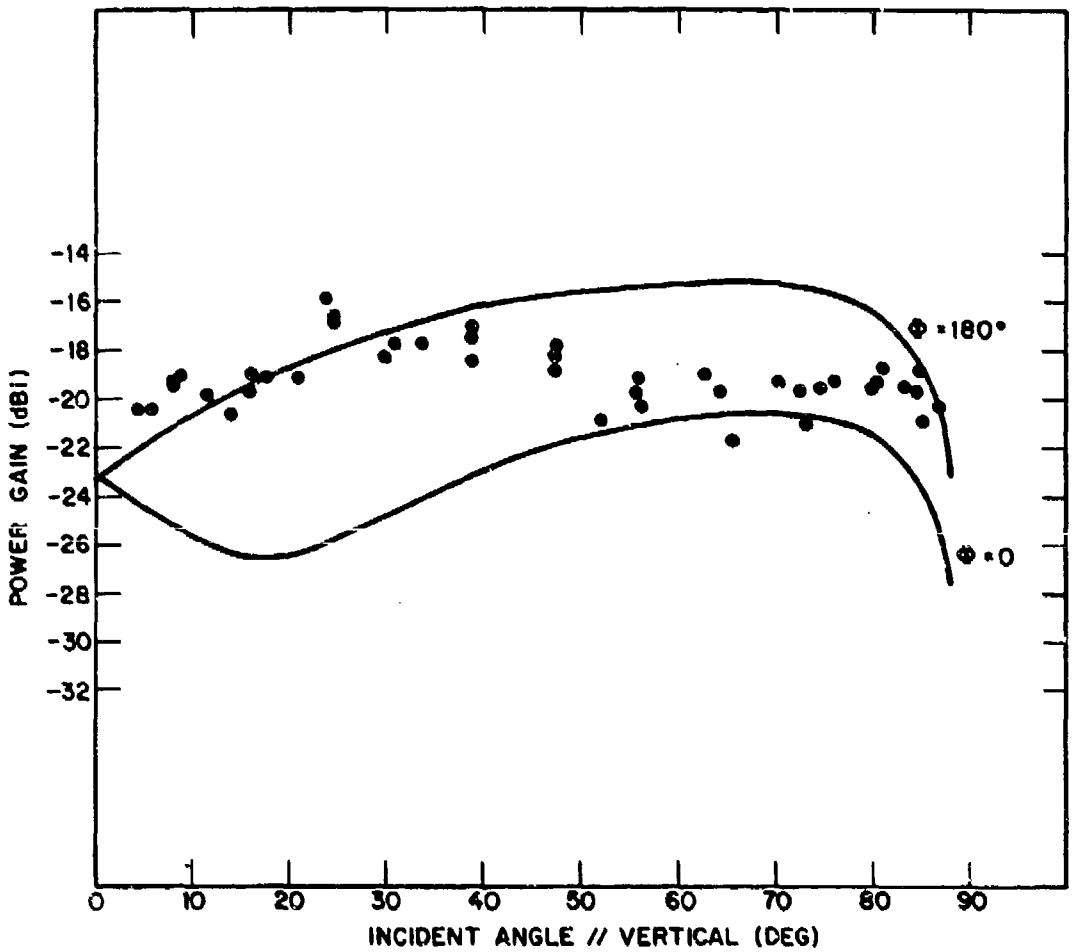

Fig. 32 — E_ϕ pattern for electrode antenna at 400 MHz (along antenna axis ($\phi = 180°$), vertical plane polarization)

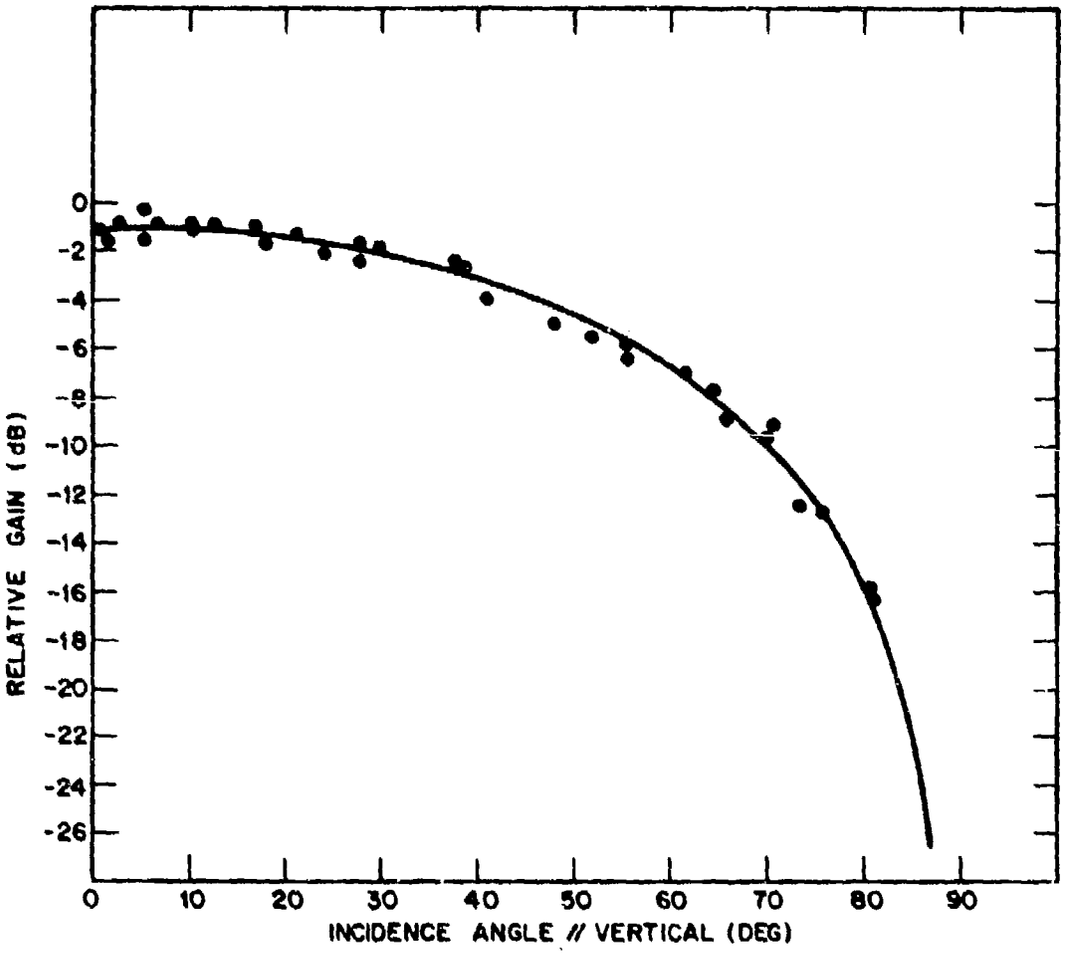

Fig. 33 — E_ϕ pattern for electrode antenna at 400 MHz (90° from antenna axis, horizontal polarization)